IAP-AACM v1.0： Global to regional evaluation of the atmospheric chemistry model in CAS-ESM

Ying Wei[1,2], Xueshun Chen[1,4], Huansheng Chen[1], Jie Li[1], Zifa Wang[1,2,4], Wenyi Yang[1], Baozhu Ge[1], Huiyun Du[1,2], Jianqi Hao[1,*], Wei Wang[3], Jianjun Li[3], Yele Sun[1], Huili Huang[1]

[1] The State Key Laboratory of Atmospheric Boundary Layer Physics and Atmospheric Chemistry, Institute of Atmospheric Physics, Chinese Academy of Sciences, Beijing 100029, China

[2] University of Chinese Academy of Sciences, Beijing 100049, China

[3] China National Environmental Monitoring Center, Beijing 100012, China

[4] Center for Excellence in Regional Atmospheric Environment, Institute of Urban Environment, Chinese Academy of Sciences, Xiamen 361021, China

[*] Now at: School of Civil and Environmental Engineering, Georgia Institute of Technology, Atlanta, GA, 30332, USA

Correspondence to: Zifa Wang (zifawang@mail.iap.ac.cn)

Abstract:

In this study, a full description and comprehensive evaluation of a global-regional nested model, the Aerosol and Atmospheric Chemistry Model of the Institute of Atmospheric Physics (IAP-AACM), is presented for the first time. Not only the global budgets and distribution, but also a comparison of nested simulation over China against multi-datasets are investigated, benefiting from the access of air quality monitoring data in China since 2013 and the Model Inter-Comparison Study for Asia

project. The model results and analysis can greatly help reduce uncertainties and understand model diversity in assessing global and regional aerosol effects on climate and human health, especially over East Asia and areas affected by East Asia. For global simulation, the 1-year simulation for 2014 shows that the IAP-AACM is within the range of other models. Overall, it reasonably reproduces spatial distribution and seasonal variation of trace gases and aerosols in both surface concentrations and column burdens (mostly within the factor of two). The model well captures spatial variation for carbon monoxide with a bit underestimation over ocean, which implicates uncertainties on ocean source. The simulations well matches the seasonal cycle of ozone except for lands in the northern hemisphere, partly due to the lack of stratospheric-tropospheric exchange. For aerosols, the simulation of fine-mode particulate matter ($PM_{2.5}$) matches observation well. The simulation on primary aerosols (Normalized Mean Bias (NMB) are within ± 0.64) is better than secondary aerosols (NMB are greater than 1.0 in some regions). For nested regional simulation, IAP-AACM shows the superiority of higher resolution simulation using the nested domain over East Asia. The model reproduces variation of sulfur dioxide (SO_2), nitrogen dioxide (NO_2) and $PM_{2.5}$ accurately in typical cities, with correlation coefficients (R) above 0.5 and NMB within ± 0.5. Compared to the global simulation, the nested simulation exhibits an improved ability to capture the high temporal and spatial variability over China. In particular, R for SO_2 and NO_2 and $PM_{2.5}$ are raised by ~0.15, ~0.2 and ~0.25 respectively in the nested grid. Based on the evaluation and analysis, model improvements needed are suggested.

Key words: IAP-AACM, model evaluation, multi-model inter-comparison, $PM_{2.5}$, China

1. Introduction

Atmospheric composition can affect climate and environment through direct and indirect effects (Intergovernmental Panel on Climate Change (IPCC), 2001). The composition of the troposphere has changed a lot due to anthropogenic activities over the past decades (Akimoto, 2003; Tsigaridis et al., 2006). Changes in the concentration of trace gases such as sulfur dioxide (SO_2) and nitrogen oxides (NO_x = NO + NO_2) have a substantial impact on acid deposition (Mathur et al., 2003), atmospheric oxidation (Calvert, 1984), and gas-particle transformation processes (Saxena et al., 1987). Aerosols formatted from these precursor gases, together with aerosols from other sources, have a direct radiative forcing. By modifying cloud properties, the aerosols also have important indirect effects. As reported in the Fifth Assessment Report (AR5) of IPCC (Myhre et al., 2013), the radiative forcing of aerosols ranges from -1.9 ~ -0.1 W m^{-2}, with the direct radiative forcing ranges from -0.85 ~ 0.15 W m^{-2}. With better model performance and more robust observation network, AR5 achieved increasing confidence in the assessment compared with AR4 (Boucher et al., 2013), but radiative forcing associated with aerosols still has large uncertainties. In addition, aerosols have adverse impacts on human health including respiratory diseases, cardiovascular risk and lung cancer, which has drawn increasing public attention (Burnett et al., 2014; Pope et al., 2011; Powell et al., 2015). It is necessary to represent the key physical and chemical parameters controlling trace

gases and aerosols in order to quantify these adverse effects and project the influence of aerosols in the future.

Chemical Transport Models (CTMs) are mathematical tools for studying the evolution of chemical constituents in the atmosphere. CTMs have irreplaceable advantages in terms of source and sink assessment of trace gases, historical process reproduction, and future scenario projection. Together with observations and laboratory simulations, CTMs have become the main methods for atmospheric environmental research (Wang et al., 2008). But there are numerous uncertain factors affecting model results (e.g. meteorology, emissions and model framework and physiochemical schemes). Therefore, model evaluation is essential for model development and scientific analysis. To date, many assessments with a single model using various observation datasets and multi-model inter-comparisons (with or without observations) have provided us with a comprehensive understanding of model performance and uncertainty. For example, Badia et al. (2017) evaluated the gas-phase chemistry of the Multi-scale Online Nonhydrostatic Atmosphere Chemistry model (NMMB-MONARCH), Mann et al. (2010) evaluated both mass concentration and number concentration of the Global Model of Aerosol Processes (GLOMAP), and Tsigaridis et al. (2014) gave a detail evaluation of organic aerosol in the Aerosol Comparisons between Observations and Models Project (AeroCom). However, evaluations against site observations mainly focused on America and Europe and it's inadequate for EA due to a limited set of data (Søvde et al., 2012; Lee et al., 2015; Kaiser et al. 2018). Spatial distribution of aerosols affects estimation of radiative

forcing (Shindell et al., 2013; Giorgi et al., 2003). Thus using more observations to assess the model results helps to reduce uncertainties of climate effect prediction over East Asia (EA).

Along with economic development and urbanization, most megacities in China have been plagued by haze in recent years. There are many reports on observation and simulation studies addressing particulate matter. The model studies mainly focus on the relationship between haze and weather conditions (Zhang et al., 2015; Tie et al., 2015, 2017), pollutants source apportionment (Wang et al., 2014; Wang et al., 2014), and chemical mechanism of particulate formation (Cheng et al., 2016). Regional models are more often used in local air pollution researches due to its advantage in capturing the variation of inputs (e.g. meteorology, underlying surface and emissions) and therefrom the temporal and spatial variation of pollutants. However, the regional models can't study the long range transport between AE and its downwind/upwind regions due to the limits of lateral (and upper) boundary conditions.

Based on the Global Nested Grid Air Quality Prediction Model System (GNAQPMS) (Chen et al., 2015), we developed the Aerosol and Atmospheric Chemistry Model of the Institute of Atmospheric Physics (IAP-AACM) and coupled it into the Earth System Model of the Chinese Academy of Sciences (CAS-ESM) as the atmosphere chemistry component of the model, using the framework of coupler 7 (CPL7) (Tang et al., 2015; Zhu et al., 2018). IAP-AACM incorporated the localization of several modules, such as dust emission and heterogeneous chemistry. For the dust module, the deflation mechanism and dust loading parameterization are based on a

detailed analysis of the meteorological conditions, landform, and climatology from daily weather records at about 300 local stations in North China (NC) (Wang et al., 2000). For the heterogeneous chemistry scheme, the parameterization of uptake coefficients improved the simulation of sulfate and nitrate in China during the severe haze period (Li et al., 2018). With the ability of multi-scale nesting, it has advantage in application in EA. The development of IAP-AACM allows us to quantify climate effects on a global scale and elucidate air pollution problems on a regional scale over China. Here a large number of datasets are used to evaluate the model, including a dataset of city sites covering China. Continuous year-round observations at city sites can help study of air pollution and model evaluation in China. As we are currently building a global forecasting platform, the model evaluation across a wide range of cities will also provide knowledge for global model forecasting and assessment.

In this study, the off-line IAP-AACM is applied to a 1-year simulation for 2014 and the model results of trace gases and aerosol mass concentration are evaluated against other model datasets and a wide range of observational datasets, including site observations and satellite data. Firstly we present the global evaluation in section 3.1~3.2. The global budgets of sulfur (dimethylsulfide (DMS), SO_2 and sulfate) and carbonaceous (organic matter (OM) and black carbon (BC)) aerosol are compared with other aerosol models in section 3.1. The global distribution and evaluation of trace gases and aerosol are shown in section 3.2. In section 3.3~3.4, we focus on the model simulation of $PM_{2.5}$ and its components in Chinese cities. The nested simulation is compared with an abundant dataset of city sites which cover most areas

in China, and the impact of different resolutions on model performance is also explored. An inter-comparison with the Model Inter-Comparison Study for Asia (MICS-Asia) models is presented in section 3.3, to give a general comparison across EA.

2. Model description and setup

2.1 Model description

2.1.1 CAS-ESM

CAS-ESM is the Earth System Model developed by the Chinese Academy of Sciences. It is a coupled model incorporating the Atmospheric General Circulation Model of IAP (IAP-AGCM) (Su et al., 2014), the Climate System Ocean Model (LICOM) (Liu et al., 2012), the Common Land Model (CoLM) (Dai et al., 2015), the sea ice model (CICE), the Dynamic Global Vegetation Model of IAP (IAP-DGVM) (Zhu et al., 2018), the IAP-AACM, and the land and ocean biogeochemical models of IAP (IAP-OBGCM) (Li et al., 2012). The IAP-AACM provides mass concentration of trace gases and aerosols for CAS-ESM and responds to the feedback of aerosols on meteorological fields. Currently, global climate and ecological environment change is not only one of the core issues of international climate and environment diplomacy, but also an important factor governing the sustainable development of China. Earth system model is a basic tool to understand and solve these problems. The resolution of the CAS-ESM is 1°×1°currently and later will be updated to 0.25°×0.25°. The CAS-ESM will be used for the climate numerical experiment with high resolution

(0.25°×0.25°) for 100 years (1950 ~ 2050) and provide simulation results for the CMIP6 and IPCC AR6.

2.1.2 IAP-AACM

The IAP-AACM is developed on the basis of the Nested Grid Air Quality Prediction Model System (NAQPMS) (Wang et al. 2006b) and the Global Nested Grid Air Quality Prediction Model System (GNAQPMS) (Chen et al., 2015). NAQPMS/GNAQPMS is widely used in the simulation of dust (Li et al., 2012), ozone (O_3) (Wang et al., 2006a; Li et al., 2007), deposition (Ge et al., 2014), air pollution policy control (Wu et al., 2011; Li et al., 2016; Wei et al., 2017) and the global transportation of mercury (Chen et al., 2015).

Like GNAQPMS, the IAP-AACM is a multi-scale nested model that describes atmospheric chemistry and aerosol process on both global and regional scales. In the IAP-AACM, sea salt and dust emissions are calculated online. The dust scheme originates from the wind erosion model developed by Wang et al. (2000) and improved by Luo et al. (2006). The simulation of sea salt is based on the scheme of Athanasopoulou et al. (2008). Dry deposition processes are based on the resistance model approach of Zhang et al. (2003). The gas-phase chemistry scheme is Carbon Bond Mechanism Z (CBM-Z) (Zaveri et al., 1999). The cloud convection, aqueous chemistry, in-cloud and below-cloud scavenging use the second generation of Regional Acid Deposition Model (RADM2) (Stockwell et al., 1997). For aerosols, the thermodynamic equilibrium module ISORROPIA (Nenes et al., 1998, 1999) is used to calculate gas-particle partitioning of inorganic aerosols and aerosol water content.

Furthermore, an aerosol microphysics dynamic module (APM) (Yu et al., 2009) was added to expand the simulation from mass concentration to size distribution (Chen et al., 2015, 2017). The secondary organic aerosol (SOA) module is based on the mechanism developed by Strader (1999), considering two anthropogenic emission precursors (toluene and other aromatic hydrocarbons) and four bio-emission precursors (isoprene, monoterpene, etc.) (Li et al., 2011).

In addition, the IAP-AACM includes an updated DMS emission module from Lana et al. (2011). The DMS concentration in seawater is calculated using 47,313 observations of the Global Surface Waters DMS database (http://saga.pmel.noaa.gov/dms/) and an additional 63 observations in the South Pacific (Lee et al., 2010). The IAP-AACM also provides simplified gas-phase chemistry mechanism specially designed for CAS-ESM to provide the major aerosol components (sulfate, OM, BC, dust and sea salt). Retaining aerosols with significant climatic radiative effects while cutting computational load, nitrate and its chemical reactions are excluded. This approach is common in global aerosol models such as the Integrated Massively Parallel Atmospheric Chemical Transport (IMPACT) model (Liu et al., 2005) and GLOMAP (Mann et al., 2010). The simplified scheme contains sulfur species (SO_2, DMS, and sulfur acid gas (H_2SO_4)), ammonia (NH_3) and hydrogen peroxide. Offline monthly fields of the oxidants hydroxyl radical (OH), nitrate ion radical (NO_3), O_3 and super oxidation of hydrogen (HO_2), generated from a simulation of the standard version of IAP-AACM, are read in and interpolated. Chemical processes in the simplified version are the same as those in the standard

version except for the gas-phase scheme mentioned above. In this paper we focus on evaluating simulation results of the standard version model driven by a global version of Weather Research and Forecasting (WRF).

2.2 IAP-AACM setup

In this study, the simulation region covers the globe at 1 °×1 ° resolution and has a nested domain over EA at 0.33 °×0.33 °. Vertically, the model uses 20 layers, from the bottom layer center of 50m to the model top of 20km, and about 10 layers are located below 3 km. The model domain is shown in Fig. 1. The synchronous time step of integration is 1800 s. The meteorology input frequency is 6 hour in the global domain but 3 hour in the nested domain. The simulation period is from December 1st, 2013 to December 31th, 2014, and the first month is spin up time. Lateral boundary conditions for the nested region are real-time calculated by the parent grid. The initial conditions and top boundary conditions of O_3, NO_x and CO are prescribed from the Model for Ozone and Related Chemical Tracers version4 (MOZART-4) (Emmons et al., 2010).

2.3 Emissions

By integrating data from publicly-released emission inventories, we compiled a global high-resolution (0.1 ° × 0.1 °) emission dataset with source categories (29 species and 14 sectors) and interpolate it to the model resolution. The benchmark year is 2010. Detailed information on the emissions is shown in Table 1. We note that volcanic emissions are not yet considered here.

As a consequence of government control policy included in the Five-Year Plan (FYP), China has achieved an obvious decrease in air pollution in the past ten years,

especially for SO_2. According to an announcement by the Ministry of Environmental Protection of China (http://www.zhb.gov.cn/gkml/hbb/qt/201507/t20150722_307020.htm), the country completed the emission reduction task of 12th FYP (2010~2015) ahead of schedule in 2014 with a reduction ratio reaching by 12.9%. As the FYP controls suppressed SO_2 emissions mainly in the energy and industry sectors, we adjusted the total SO_2 emission for 2014 by a factor of 0.9 in China. The annual mean SO_2 emission is shown in Fig. 1. According to the latest emission inventory study for China (Zheng et al., 2018), the other species of emissions didn't decrease so much from 2010 to 2014. Thus we didn't modify the other emissions.

2.4 Meteorology and evaluation

Meteorological fields were provided offline by the global WRF. The global WRF is an extension of mesoscale WRF that was developed for global weather research and forecasting applications. It has more general choice of map projection (to include both conformal and non-conformal map projections). The specification of planetary constants, physics parameterizations and timing conventions are also improved to allow the model to be run as a global model. Thus, it has multiscale and nesting capabilities, blurring the distinction between global and mesoscale models and enabling investigation of coupling between processes on all scales (Richardson et al., 2007). In the study we used WRF version 3.3 (WRFv3.3). The temporal and horizontal spatial resolution of WRFv3.3 was consistent with IAP-AACM. The atmosphere was divided into 27 vertical layers up to 10 hundred Pascal (hPa). Output

of WRF is interpolated to the vertical layers defined in IAP-AACM. WRF was driven by the National Centers for Environmental Prediction (NCEP) Final Analysis (FNL) data and the calculation is nudged to the FNL data.

A comparison of annual mean meteorological fields (temperature, wind and relative humidity) between WRF and reanalysis data (NCEP Reanalysis 1) are presented in Fig. 2. A comparison of annual mean precipitation between the model and reanalysis data from the Global Precipitation Climatology Project is also shown in Fig. S1. Globally, as shown in Fig. 2, the difference in temperature at 2 m (T_2) and wind at 10 m (W_{10}) between the model and observation is within 2 ℃ and 2 m s^{-1} respectively, except in high-latitude areas. The relative humidity at 2 m (RH_2) is generally underestimated on land and overestimated over the ocean, the difference in most areas is within ±10%. The difference in precipitation is within 2 mm day^{-1} except equatorial regions. The frequently strong convection in tropical areas is difficult to reproduce in the model. 443 surface sites in the nested domain are also analyzed with the National Climate Data Center (NCDC) data and the statistical parameters are shown in Table 2. The simulation of the meteorological factors are close to the site records in different season, with mean bias (MB) of -0.3 ~ 0 ℃, -0.8 ~ -0.5 m/s and -4~ -2.3% for T_2, W_{10} and RH_2 respectively. The model underestimates T_2 in all the seasons, especially in summer with Root Mean Square Error (RMSE) of 2 ℃. As for W_{10}, it's also underestimated with MB of -0.8m/s. As for RH2, the underestimation is more obvious in summer (MB= -3.2%) and autumn (MB= -3.2%) than in spring (MB= -2.3%) and winter (MB= -2.8%), mainly stem from the

insufficient prediction of precipitation. The agreement in T_2 and RH_2 with observations is better than that of W_{10}, with annual correlation coefficients (R) of 0.98, 0.84 and 0.53, respectively. Generally, the meteorology calculated by WRF can rationally reproduce the characteristics of observations.

2.5 Observation data

Trace gas observation data for CO, O_3, SO_2, and NO_2 in this paper are collected from the World Data Center for Greenhouse Gas (WDCGG) (http://ds.data.jma.go.jp/gmd/wdcgg/cgi-bin/wdcgg/catalogue.cgi), the Acid Deposition Monitoring Network in East Asia (EANET) (http://www.eanet.asia/product/index.html#datarep), and the Chinese National Environmental Monitoring Center (CNEMC) (http://www.cnemc.cn). Annual observation data of particle and aerosol species are from the European Monitoring and Evaluation Program (EMEP) (http://www.emep.int/), EANET, the United States Environmental Protection Agency (EPA) (http://aqsdr1.epa.gov/aqsweb/aqstmp/airdata/download_files.html#Daily) and the Interagency Monitoring of Protected Visual Environments (IMPROVE) network (http://vista.cira.colostate.edu/improve/). As there is no data published for BC and organic carbon (OC) in Asia in 2014, we collected earlier records from the China Atmosphere Watch Network (CAWNET) reported by Zhang et al. (2008). Hourly air quality data in China are downloaded from CNEMC. The other aerosol observations in China are collected from monitoring sites of Nanjing and Wuhan, and scientific observation at Xinzhou and Beijing (Chen et al., 2015). Aerosol Optical Depth (AOD)

product of MYD04_L2 (http://dx.doi.org/10.5067/MODIS/MYD04_L2.006) from the Moderate Resolution Imaging Spectroradiometer (MODIS) is used to evaluate the simulated AOD. Total column product from the Global Ozone Monitoring Experiment 2 aboard METOP-A (GOME-2A) (https://www.ospo.noaa.gov/Products/atmosphere/gome/gome-A.html) and the Ozone Monitoring Instrument (OMI) (https://earthdata.nasa.gov/earth-observation-data/near-real-time/download-nrt-data/omi-nrt) are also used to evaluate the vertical tropospheric column (VTC) of NO_2 and O_3, respectively. All these datasets are for 2014, except that the CAWNET is for 2006. The corresponding simulations at observation sites are sampled at model grid cells containing those sites. The simulation of seasonal cycle in different regions or cities are first sampled at the model grid cells containing the observational sites and then averaged within sub-regions. The observation datasets are summarized in Table 3 and detailed information for observation sites is given in Table S1. Note that the observed species in Table 3 are not always available at the corresponding sites.

To investigate the model performance over China, we selected 89 stations in 12 cities representing typical areas (NC, Yangtze River Delta (YRD), Pearl River Delta (PRD), Northwest China (NWC), Central China (CC), Southwest China (SWC)) in China (shown in Fig. 1). The six regions represent the major geographical regions over China and they are also the regions on which severe air pollution researches focus. The daily mean city-averaged concentration of pollutants are displayed in figures and used to calculate statistics. In addition, we collected the mass

concentrations of BC, OM, sulfate, nitrate and ammonium in Beijing, Xinzhou, Nanjing and Wuhan (shown in Fig. 1) to evaluate the model performance in simulating aerosol components.

3 Model results and evaluation

3.1 Budgets

On account of the significant radiative effect of sulfate and carbonaceous aerosols, their budgets play an important role in the climate change (Penner et al., 1998). Here we elucidate the budgets of sulfate with its precursor gases (DMS and SO_2) and carbonaceous aerosols.

The global budgets for DMS, SO_2 and sulfate in IAP-AACM are summarized in Table 4. For comparison, Table 4 also lists results from other global aerosol models including IMPACT (Liu et al., 2005), Goddard Institute for Space Studies General Circulation Model with TwO-Moment Aerosol Sectional (GISS-TOMAS) (Lee et al., 2010), Atmospheric Chemistry and Climate Model Intercomparison Project (ACCMIP) models (Lee et al., 2013) and the AeroCom models (Textor et al., 2006). The DMS emission (23.3 TgS yr^{-1}) of IAP-AACM is within the range of other models (10.7~22.8 TgS yr^{-1}). The dry deposition of DMS is zero in IAP-AACM. Therefor the sink is only oxidation. This treatment is common in other models such as ModelE2-TOMAS and ModelE2-OMA (Lee et al., 2015). As a result, we have a higher burden of DMS of 0.19 TgS, just outside the range (0.05~0.15 TgS), and a longer lifetime of 3 days. For SO_2, the emissions are a bit lower than the reference range (54.3 TgS yr^{-1} vs. 63.4~94.9 TgS yr^{-1}). This is ascribed to the lack of volcanic

emissions. The volcanic emissions of SO_2 is about 12.5 TgS yr^{-1} used in most models, based on the work of Andres and Kasgnoc (1998) and Dentener et al. (2006). The oxidation of DMS to SO_2 is 22.8 TgS yr^{-1}, within the range of other models' results. The aqueous-phase process is responsible for 61% of the oxidation to sulfate and gas-phase processes are responsible for the remaining 39%. Although it's a bit lower conversion efficiency for aqueous-phase chemistry compared with other models (about 70% ~ 80%), both aqueous phase and gas phase oxidation are well within the range of other models. Due to the lower removal in aqueous-phase oxidation (29.8 Tg S) and wet deposition (as zero), the lifetime of SO_2 in the model is a little longer than other models (3 days vs. 0.6~2.6 days). In IAP-AACM, the emission of H_2SO_4 is assumed as 2.5% of the total sulfur emission. With a strong wet scavenging effect, 94% of sulfate is removed by wet deposition and the rest by dry deposition.

Table 5 lists the budgets for BC and OM in IAP-AACM. They are in the range of results from other models including Liu et al. (2005), Lee et al. (2013), Lee et al. (2015), Textor et al. (2006), and those listed in Liu et al. (2005). The emissions of BC/OM are at the low end compared with other models (BC: 7.42 TgS yr^{-1} vs. 7.4~19.0 TgS yr^{-1}; OM: 56.7 TgS yr^{-1} vs 34~144 TgS yr^{-1}). The ratio of dry deposition to wet deposition for BC and OM is 15.8% and 13.6%, respectively. Both the burden and lifetime of carbonaceous aerosol are within the other models' results. The burden of BC and OM is 0.13 Tg and 1.16 Tg respectively and the lifetime is 6.4 days and 7.4 days respectively.

The budgets for CO and O_3 are displayed in Table S2. As for CO, the total

emissions are 994 Tg yr^{-1} in IAP-AACM. It's smaller than those in the other models (e.g., 1159 Tg yr^{-1} in Huijnen et al. (2010), 1210.7 Tg yr^{-1} in Emmons et al. (2010)). Direct emissions and oxidation contribute 43.4% and 55.4% to the total CO, respectively. The global annual burden is 327 Tg, smaller than the other models of 353~399 Tg (Horowitz et al., 2003; Huijnen et al., 2010; Badia et al., 2017;). As for ozone, dry deposition contributes 21.3% to the total loss (4924 Tg yr^{-1}), and photochemical reaction is responsible for the rest loss. The dry deposition (1049 Tg yr^{-1}) is larger than values of model collection of ACCENT and ACCMIP (Young et al., 2018).

3.2 Global distribution and evaluation

3.2.1 Hydroxyl radical (OH)

Oxidation is the basic characteristic of atmospheric chemistry. As the most important oxidant in atmosphere, OH is the crucial species in CTMs. OH in troposphere is mainly produced by the reaction O_3 + *hv* (λ≦320nm) + H2O → 2OH+O2. The tropospheric mean concentration of OH in IAP-AACM is 13.0×10^5 molec cm^{-3}. It is a little higher than the mean OH concentration ($11.1\pm1.6\times10^5$ molec cm^{-3}) given by 16 ACCMIP models in Naik et al. (2013). The high concentration indicates a stronger atmospheric oxidation. This could explain the lower concentration of CO over ocean. The zonal mean OH concentrations for January, April, July and October are shown in Fig. 3. Like other chemistry models, OH concentration in the tropics keeps highest all the year round and decreases gradually from tropics to poles. This is due to the positive influence of solar radiation and water vapor concentration.

The seasonal north-south shift of OH maximum area is also ascribed to the seasonal variation of these two factors. The mean inter-hemispheric (N/S) ratio of OH in the model is 1.26, in accordance with the multi-model mean ratio of 1.28±0.1 (Naik et al., 2013). Vertically, the highest concentration is in the layer of 2-4 km over the tropics. In Northern Hemisphere, the highest OH concentration appears in summer. Peak value is located at around 30°N, in the atmosphere above 2km. Generally, the distribution of OH concentration is similar with other models (Huijnen et al., 2010; Badia et al., 2017).

3.2.2 Trace gases

Global annual-averaged surface-layer trace gas distributions from IAP-AACM are evaluated against site observations in Fig. 4(a). Scatter plots of observations and simulations divided into 11 regions are exhibited in Fig. 4(b). Fig. 5 shows the comparison of annual surface concentrations of CO, O_3 and NO_2 between IAP-AACM and HTAP CTMs including CAM-Chem (Lamarque et al., 2012), OsloCTM3 (Søvde et al., 2012), and CHASER(Sudo et al., 2002).

Overall, the global surface CO simulation of IAP-AACM is lower than observations, especially in natural source regions. The difference over ocean reaches ~100 ppb, with NMB ranging from -0.59 to -0.45 shown in Table S3. In anthropogenic source regions, the model is close to site records in North America (NAmerica), EA, and Europe with NMB of -0.23, -0.34, -0.39 respectively. The scatter plot clearly shows a negative bias between the model and observations. The lower model results should be related to underestimated emissions and overestimated

OH. As discussed in Sect. 3.2.1, the OH concentration in troposphere is slightly higher than the other models. As shown in Fig. 3, in IAP-AACM, the peak concentration of OH (30-35 molec cm^{-3}) is higher than the other models (under 30 molec cm^{-3}). Due to the sink reaction of CO ($CO + OH \rightarrow CO_2 + H$), the CO loss is larger in IAP-AACM. Moreover, the anthropogenic emission of CO is 546.4 Tg yr^{-1} in IAP-AACM (shown in Table S2). It's lower than other emission inventory (e.g. MOZART-4 with 642 Tg yr^{-1} (Emmons et al., 2010), ACCMIP with 610.5 Tg yr^{-1} (Badia et al., 2017)). Janssens-Maenhout et al. (2015) pointed out that CO emission from HTAPv2 has an uncertainty of 15~100% and 35~150% in data from well maintained countries and poorly maintained countries respectively. Furthermore, Shindell et al. (2006) evaluated 26 global models and showed that all the model results are lower than observations in the Northern Hemisphere (NH) except in the tropics. It's related to a lower CO emission source. The spatial distribution of CO concentrations in IAP-AACM is similar to that in other models from HTAP in 2010. High values are found in industrial areas such as NAmerica, Europe and EA, and biomass burning areas (BBAs) such as South Africa (SAfrica) and South America (SAmerica). Overall, IAP-AACM shows lower concentration in BBAs. The difference probably relates to the different fire emissions used in IAP-AACM and HTAP models (GFED4 vs. GFED3) (Janssens-Maenhout et al., 2015). Due to the impact of a reduction of combustion area and decreasing in fuel consumption, there is a reduction of about 20%~30% in BBAs for CO emissions in GFED4, compared with GFED3 (Werf et al., 2017).

The surface distribution of O_3 simulated by IAP-AACM is in a good agreement with observations. The O_3 simulations at most sites are within a factor of two of observations and all the regions have NMB within ±0.2 (Table S3) except for Antarctica and Asia. There are three sites in Southeast Asia exhibit concentrations more than twice the observed values. As the sites are located at coast, simulations in the coarse grids can't capture the steep variation. Besides, South Asia is a high-emission area for biogenic VOCs. Uncertainties in the biogenic emission inventory also cause large errors in O_3 simulation due to photochemical processes. As shown in Fig. 5, IAP-AACM exhibits generally similar surface distribution of O_3 to the other models. But the model shows lower concentrations in high-latitude areas (especially over ocean) than the other models. That should be partly related to the dry deposition over sea ice. The dry deposition velocity to ice is under 0.02 cm s^{-1} across 15 HTAP models (Hardecre et al., 2015). In IAP-AACM, it's higher (0.035~0.048 cm s^{-1}) than those models, as shown in Fig. S2. Additionally, the dry deposition velocity over ocean is 0.042~0.05 cm s^{-1} in IAP-AACM. compared with the HTAP models (around 0.05 cm s^{-1}), there should be a difference less than 12% according to the research in Ganzeveld et al. (2009).

As shown in Fig. 6, the model shows a good skill in capturing the seasonal variation of surface O_3 in the Southern Hemisphere (SH) and the NH oceans. Over ocean, O_3 concentration is higher in spring and lower in summer. In contrast, it's higher in autumn or summer in the SH land. The model shows poor performance on seasonal cycle of surface ozone in the NH, with underestimation in NH land in cold

seasons and overestimation in Europe and EA in summer. In IAP-AACM, the stratospheric-tropospheric exchange is not considered. It leads to a large negative bias in the simulation. The stratosphere-to-troposphere ozone transport event occurs widely across mid-latitudes in the NH (Monks et al., 2000; Akritidis et al., 2018). Researches (Munzert et al, 1985; Austin and Follows, 1991) showed that the maximum of stratosphere to troposphere flux occurs in late winter/spring. The surface O_3 concentrations over EA (sites mainly located in Japan) are overestimated in summer and early autumn. The same pattern is also found in the multi-model inter-comparison of 21 HTAP models (Fiore et al., 2009). The simulations in island countries of EA are sensitive to the timing and extent of the Asian summer monsoon (Han et al., 2008). The positive model bias in this season may stem from inadequate representation of southwesterly inflow of clean marine air. Furthermore, the underestimation of cloud cover in summer may also responsible for the overestimation of O_3 due to stronger photochemistry. Additionally, it's difficult for global model with coarse resolution to resolve local orographically driven flows or sharp gradients in mixing depths under complex underlying surface conditions in lands. As the seasonal variation of surface O_3 should be different in different environment, a seasonal cycle comparison with these NH sites which are separated as land, mountain and marine are also shown in Fig. S3. To varying degrees, the underestimation in cold seasons and overestimation in summer are found in different environments. For inland, the model tends to overestimate O_3 concentrations in summer time. Uncertainties in volatile organic compounds (VOCs)-NOx-O_3

chemistry may contribute. The natural source of isoprene from vegetation is important in the O_3 formation due to its high proportion of VOCs emission in summer (as estimated to be 40.9 Tg/yr in China by Fu et al., 2012). In IAP-AACM, ozone concentration is about 5~15 ppb lower than site observations in Antarctica. It may be caused by the lack of halogen chemistry in the model. Remarkable ozone depletion events which is driven by halogen chemistry (mostly notably as bromine) is observed in the polar boundary layer (Simpson et al., 2007). The model study by Falk & Sinnhuber (2018) indicated that there are missing sources of bromine release from ice and snow in EMAC v2.52. The over prediction of dry deposition velocity to sea ice also plays a role here, as aforementioned discussion.

NO_2 mainly distributes in the anthropogenic source areas, which is well captured by IAP-AACM, see Fig. 4(a). In the NH, the maxima are located in urban areas due to fossil fuel combustion in traffic and industry. The surface concentration of NO_2 is much higher in eastern China (>20 ppb) than that in eastern NAmerica and Europe (3-10 ppb). In the SH, the maxima are located in SAmerica and SAfrica due to biomass burning, where NO_2 ranges of 1-10 ppb. The simulations are in good agreement with observations in NAmerica, Europe, and most parts of EA. As shown in Fig. 4(b), simulations are within a factor of two of observations at most sites, with NMB of -0.14, 0.16 and -0.14 for Asia, Europe and NAmerica, respectively. As we use the same anthropogenic emission inventory, the distribution of NO_2 in NH between IAP-AACM and other models is similar (shown in Fig. 6). The concentration in in SAmerica and SAfrica is slightly lower (~3 ppb) than the other models, due to

aforementioned different version of GFED data used in IAP-AACM and HTAP models. Compared with the other models, the surface NO_2 over ocean is larger in IAP-AACM. In IAP-AACM, the emissions of energy and industry are emitted in the first five layers considering the stack height. The higher injection height of emissions leads to further transportation distance and lower NO_x at surface of source areas (Badia et al., 2017). Consequently, it also leads to higher concentration of surface ozone in NH source areas due to weak NO_x titration.

Similar to NO_2, SO_2 shows high value in the NH land, mainly due to human activities associated with fossil fuel combustion. Maximum concentrations are mainly found in NAmerica, Europe, India and EA, ranging of 5-20ppb. It's even over 20 ppb in Eastern China. SO_2 over ocean is mainly due to DMS oxidation from marine organisms, ranging of 0.1-1ppb. The model shows a distribution of 0.1-20 ppb in EA and 0.1-5 ppb in western NAmerica, which is consistent with observations. The simulation of SO_2 in eastern NAmerica and Europe is about 1-10 ppb, which are overestimated with NMB=3.51 and NMB=3.79 respectively, as shown in Table S3.

3.2.3 Aerosol composition

Fig. 7 shows the annual surface concentrations of aerosols in IAP-AACM in comparison with site observations. The formation of sulfate, nitrate and ammonium (SNA) are due to gas-to-particle conversion in the atmosphere. The distribution of SNA are consistent with the precursor gases (SO_2, NO_x, NH_3), mainly in the NH land. As shown in Fig. 7(a), the surface distribution of SNA in IAP-AACM is close to the site records generally. As shown in Fig. 7(b), sulfate is overestimated more or less.

Specifically, in Asia, the simulations at most sites here are within a factor of two of observations, with NMB of 0.36. However, In NAmerica and Europe, it's overestimated with NMB of 1.94 and 1.1 respectively. The sites average simulation is 1.67 μg m^{-3} and 1.56 μg m^{-3} higher than observations in NAmerica and Europe respectively. The overestimation is consistent with the high level of SO_2 described previously. There are more uncertainties in the simulation of nitrate. Since the volatility of HNO_3 makes nitrate formation more sensitive to environmental factors such as temperature and relative humidity in the atmosphere. The complex photochemical reactions of NO_x also contribute to the uncertainties. The concentration of nitrate is higher in eastern America and lower in western America. IAP-AACM reproduces the distribution of nitrate in western America well but overestimates it in eastern America. The model doesn't fully capture the spatial variation over Europe, with an overestimation at most of the sites. For EA, there is an underestimation of ~5 μg m^{-3} in Southeast Asia and Japan. Overall, the NMB are within ±0.8 (as 0.5, 0.74 and -0.61 for NAmerica, Europe and EA respectively). The performance of ammonium varies in different regions since there are more uncertainties in the emission of NH_3 (precursor of ammonium) from croplands (Xu et al., 2019). There is slight negative bias in America and positive bias in Asia, with NMB less than ±1 (-0.46 and 0.85 respectively). In Europe, there is significant positive bias with NMB of 1.49.

Due to the large contribution of biomass burning and fossil fuel combustion with old technology, carbonaceous aerosols are higher in developing countries than in

developed regions such as NAmerica and Europe. The concentration of BC and OC ranges 2-10 μg m^{-3} and 5-10 μg m^{-3} respectively in China and India, while it ranges ~1 μg m^{-3} and 3-10 μg m^{-3} respectively in SAfrica and SAmerica. By and large, the model results are consistent with observations in the three regions shown in Fig. 7, with the NMB within ±0.65 and ±0.7 for BC and OC respectively. The accuracy of the simulation mainly depends on emissions and deposition processes, since BC is quite inert to chemical reactions.

The simulation of BC in China is accurate with 70% of the stations within a factor of two of observation while OC is underestimated by about 5-10 μg m^{-3}. The meteorological conditions and emission inventories in the model are inconsistent with the observation year (2006) of carbonaceous in China. This may be partially responsible for the bias of OC. According to recent study, there is a slightly increasing (less than 0.1Tg) of both BC and OC emissions from 2006 to 2010 in China (Lu et al., 2011; Fu et al., 2012). As shown in Fig. 7, the simulation of BC at most sites are close to observations while the simulation of OC is significantly underestimated. The study by Fu et al. (2012) showed a significant underestimation of OC emissions over China. Furthermore, Zhao et al. (2016) found that the pathway of intermediate volatile organic compounds (IVOC) to SOA is very important for the formation of SOA. Their model experiments suggest that IVOCs constitute over 40% of OM concentrations in Eastern China. Yang et al. (2018) also showed the significant increase of SOA concentration in an observation-based box model which included the IVOCs reactions. IVOC reactions are not included in our SOA module. The SOA

module in IAP-AACM is Two-Product scheme. Model studies with Two-Product scheme estimated an underestimation of OM by 40-78% in China (Lin et al., 2016; Han et al., 2016). Thus the closely simulating of BC but greatly underestimating of OC requires an improvement in SOA formation mechanism in IAP-AACM.

Generally, the model shows good skill in simulating $PM_{2.5}$. Model results at most sites are close to observations as shown in Fig. 7(b), especially in Europe and Asia with NMB of -0.35 and -0.36 respectively. The underestimation in western China should be related to uncertainties in emissions and unrepresentative simulation with coarse grids.

3.2.4 Comparison with satellite data

The VTC of O_3 is compared against satellite observation derived from OMI (shown in Fig. 8). In the main board, the pattern of the seasonal cycle was covered by the model. In mainland of Northern Hemisphere, the higher O_3 VTC appears during June-July-August (JJA), while in SH, it appears during September-October-November (SON) with a range of 40-60 DU. The model keeps a high value (40-50 DU) in tropics during December-January-February (DJF), possibly due to the high concentration of CO emit from biomass burning. The underestimation of cloud cover in the Intertropical Convergence Zone may contribute, too. The O_3 VTC is significantly underestimated over ocean in middle-high latitudes. As the stratospheric chemistry is not considered in IAP-AACM， the lack of stratospheric-tropospheric exchanges should partly be responsible for the underestimation of column burden.

The VTC of NO_2 is also compared against satellite observation derived from

GOME-2A (shown in Fig. 9). The NO_2 VTC has a range of 20-150 $\times 10^{14}$ molecule cm^{-2} in most source areas. By and large, IAP-AACM reproduced the magnitude in different regions. In addition, the model captured seasonal variations of NO_2 concentration in the vertical troposphere well. In anthropogenic source areas of NH (e.g., NAmerica, Europe, EA), the NO_2 VTC is higher in SON and DJF while lower in JJA. The column concentration is higher during JJA in SAmerica and SAfrica, while it is higher during DJF in central Africa, due to the vegetation burning in dry season. Compared with GOME-2A, IAP-AACM showed a larger column concentration over ocean. The overestimation is also reflected in the comparison of surface concentration. This is probably caused by insufficient oxidation to nitrate and a higher injection height of emission which leads to a farther transportation distance as suggested in Badia et al. (2017). Generally, the distribution of tropospheric NO_2 by the model is consistent with satellite observation.

In order to evaluate the column burden of aerosol in IAP-AACM, we compared the AOD from IAP-AACM with MODIS satellite data as shown in Fig. 10. The calculation of light-extinction coefficient, b_{ext550} (1/Mm, at 550nm), follows equation (1) given by Li et al. (2011):

$$b_{ext550} = 3.0\times f_{SNA}(RH)\{[(NH_4)SO_4]+[(NH_4)NO_3]\}+4.0\times[OC] \\ +10.0\times[BC]+1.0\times[FD]+0.6\times[CD]+1.7\times f_{SS}(RH)\times[SS] \quad (1)$$

where $f_{SNA}(RH)$ and $f_{SS}(RH)$ represent the hygroscopic growth factor for SNA and sea salt respectively, and the variables in brackets are the mass concentration of aerosol species (OC: organic carbon; BC: black carbon; FD: fine dust; CD: coarse dust; SS: sea salt).

In Fig. 10, the model reproduces the spatial features of AOD exhibited by satellites globally. For example, the high value around 60 ℃S, ranging from 0.1 to 0.3, is due to high concentrations of sea salt. The maximum in SAmerica and SAfrica is due to the large amount of carbonaceous aerosol produced by biomass burning. The desert maximum over 0.5 is caused by mineral dust in NAfrica, Arabian Peninsula and western China. High AOD in NAmerica, Europe, India, and EA is caused by anthropogenic aerosols. Furthermore, there is a good agreement of the seasonal variations with satellite observations. For example, the AOD in the desert areas of NH reaches a maximum in March-April-May (MAM) since there are frequent dust storms in the period. SAmerica and SAfrica exhibits the highest AOD during JJA as there is more biomass burning in this season. However, there are several biases between model and observation. The model shows a weaker AOD in Southeast Asia than observation where the value is mainly controlled by biomass burning. The AOD from IAP-AACM is lower than observation to about ~0.4 in eastern China, mainly due to the negative bias in anthropogenic aerosols simulation. Furthermore, the underestimation of RH2 in eastern China (shown in Fig. 2) is also responsible for the lower simulation of AOD. The comparison of monthly gridded average AOD (shown in Fig. S4) shows a discrepancy in EA, due to the bias of dust simulation in spring.

3.3 Nested simulation evaluation

3.3.1 Distribution of pollutants in EA

Fig. 11(a) shows the annual distribution of the four pollutants SO_2, NO_2, PM_{10} and $PM_{2.5}$, against 45 city stations from the nested simulation. In general, the

simulation shows better agreement with sites in Eastern China than Western China. The distribution of $PM_{2.5}$ and its precursors show high levels in Eastern China and low in Western China, which is related to large emissions in the east. The simulation is in good agreement with observations at most sites. Concentrations of precursor gases and particles in Tibet are greatly underestimated. Because the model's coarse resolution can't represent the emission for the city. As shown in Fig. 11(b), model results for NO_2, SO_2 and $PM_{2.5}$ are mostly within the factor of two, with NMB within ± 0.3. The "NO_2" values reported by routine monitoring sites are NO_2^*, which partially includes HNO_3 and NO_3^-. It implicates that the model may overestimate "NO_2". PM_{10} concentrations are underestimated at all sites with NMB of -0.51. The model results of PM_{10} and $PM_{2.5}$ include primary $PM_{2.5}$, BC, POA, SOA and SNA. As natural dust contributes a lot to particles in Northwest China, it's underestimated in this area.

Model inter-comparison can give some insights into model uncertainties. Here a comparison between IAP-AACM and several regional models of MICS-Asia is presented in Fig. 12. The MICS-Asia models shown here are WRF-Chem(v3.9) (Tuccella et al., 2012), CMAQ(v4.7.1) (Mebust et al., 2003) and NAQPMS (Wang et al., 2006b). The simulations are for 2010 with the same meteorological fields, emissions and horizontal resolution (45 km). Overall, the IAP-AACM shows similar annual distribution as MICS-Asia models in EA, as the emission inventories used in IAP-AACM are largely the same as MICS-Asia models. The simulation of SO_2 in IAP-AACM is similar to WRF-Chem and CMAQ. The simulation of NO_2 in

IAP-AACM is lower in source area (e.g., eastern China, Japan) but higher over downwind areas, compared with CMAQ. It's possibly related to the higher injection height in IAP-AACM. Although using the same dynamic framework, SO_2 and NO_2 in IAP-AACM are lower than NAQPMS. It should be related to the different dry deposition scheme as Zhang et al. (2003) and Wesely (1989) used in IAP-AACM and NAQPMS respectively. Furthermore, the $PM_{2.5}$ from NQAPMS is higher than IAP-AACM in Northwest of China because it includes dust aerosol in NQAPMS. Overall, the simulation in the nested domain of global model is comparable to regional model.

3.3.2 Trace gas evaluation in cities

To get deeper insight into the performance of IAP-AACM in cities, the nested simulation was compared with daily averaged observations in 12 cities across China. We first focus on NO_2 and SO_2 since they are precursors of SNA aerosols. The monthly variation of SO_2 and NO_2 against observations is shown in Fig. 13 and Fig. 14. Three-quarters of cities show an annual concentration of SO_2 of around 25 $\mu g\ m^{-3}$, only a half of NO_2 in summer and autumn, owing to the strict SO_2 emission reduction policy implemented since 2005. For SO_2, the model shows good agreement with observations except in Wuhan. This probably implies an overestimation of emissions in this city. Furthermore, IAP-AACM reproduces the seasonal variation well, showing good comparison to observations with R over 0.5 in most cities as shown in Table 6. In particular, the cities in NC have a high R of 0.76-0.89.

As illustrated in Fig. 14, the model shows a good performance for NO_2 in cities of

PRD and SWC, matching observations well with RMSE less than 20 μg m^{-3}. The model captures the daily variations well with R of 0.49-0.7 in NC, YRD and PRD. However, the model overestimated NO_2 in NC, YRD and CC in summer. The overestimation of NO_2 in summer is associated with deposition removal process and multiphase chemistry in IAP-AACM. The overestimation of NO_2 and underestimation of nitrate in daytime of summer and autumn relates to over decomposition of nitric acid (HNO_3) at high temperature condition in the thermodynamic equilibrium module. Moreover, heterogeneous chemical reactions in the model should partly be responsible for the overestimation in summer. The heterogeneous chemical module coupled in IAP-AACM has been applied in North China in winter (Li et al, 2018). The mechanism significantly improved sulfate simulation under highly polluted conditions (contributing 50%-80% of total concentration of sulfate) and reduced the overestimation of nitrate. However, the simulations excluded heterogeneous chemical processes showed better performance of NO_2 (shown in Fig. S5). It indicates that a more reasonable mechanism should be considered in model development. Here we also give a comparison of NO_2 VTC over the nested domain between the model and GOME-2A in Fig. S6. Generally, the model captures seasonal variations of NO_2 VTC well. In China, the NO_2 VTC is higher during SON and DJF while lower in JJA, due to unfavorable diffusion conditions and weaker photochemical reactions in autumn and winter.

3.3.3 Aerosol composition evaluation in cities

As shown in Fig. 15, the model performs very well in the simulation of $PM_{2.5}$.

The model reproduces $PM_{2.5}$ variation over the 12 cities well, particularly in NC, YRD and SWC, with an R of 0.70-0.79, 0.71-0.80 and 0.77 respectively. The model results are close to or slightly lower than site observations with city averaged NMB of -0.12. The concentration in NC in winter days is below the observations. Underestimation of $PM_{2.5}$ in severe haze periods is common in CTMs, mainly as a result of the deficiency in the simulation of SNA and Secondary Organic Aerosol (SOA) (Zheng et al., 2015; Donahue et al., 2006). Additionally, the simulation of meteorology (e.g., RH, wind speed, planetary boundary layer height) is more uncertain in severe haze periods. There is a clear underestimation in PRD and Urumqi where mean values are less than half of the observations, with NMB around -0.5. For PRD, it should be related to the underestimation of precursor emission and decomposition of HNO_3. For Urumqi, it should be more related to the unrepresentative simulation with coarse grids. Compared with the scale of urban area and local emissions in Urumqi, the model grids area is too large. Thus the averaged value of grids is significant lower than the local site records. Furthermore, dust is an important component of $PM_{2.5}$ in Urumqi, and this is not included in the result.

To assess the performance of IAP-AACM in representing aerosol components, we compared the model results with 4 stations in NC, YRD and CC in Fig. 16. Generally, the model represents the variation of BC well with R ranging from 0.5 to 0.8 and the values are close to observations. As primary specie, its simulation depends on emission inventory and meteorological conditions. Unlike BC, OM is underestimated at these stations, with a negative bias of 8-12 μg m^{-3}. For SNA

aerosols, sulfate is close to observations in the northern cities (Beijing and Xinzhou), but is underestimated in southern and central cities (Nanjing and Wuhan) by about 10 μg m^{-3}. As the concentration of SO_2 in Wuhan is overestimated, this suggests the underestimation of transportation or the insufficient oxidation of sulfate. The insufficient conversion has been discussed widely in recent years (Cheng et al., 2016; He et al., 2014). Moreover, SO_2 emitted by coal power plants plays a vital role in the formation of sulfate. The coarse grid resolution is insufficient to reproduce the rapid conversion of H_2SO_4 to particles in the plume. The gas-phase oxidation (SO_2 + OH → H_2SO_4(g)) is very sensitive to meteorological variables (particularly radiation and temperature) and gas (OH and NOx) concentration around the stacks (Stevens et al., 2012). The results for ammonium show similar characteristics. The simulation of nitrate is highly underestimated with a difference of 6-16 μg m^{-3}. The underestimation is due to a high frequency of 'zero' value in daytime in summer and autumn. As discussed in 3.3.2, this is caused by over decomposition of HNO_3 in high temperature in the thermodynamic equilibrium module. Schaap et al. (2011) found the same phenomenon in the LOTOSEUROS model using ISORROPIA and recommended improvements in the equilibrium module, including coarse mode nitrate.

3.4 Global versus regional results

High-resolution helps improve CTMs performance, but it is limited by the applicability of parameterization schemes of physical and chemical processes. Recently, sensitivity to horizontal grid resolution has been discussed in some model studies. Wang et al. (2014) showed a better simulation of particles in North China

with CMAQ when increasing the resolution from 36km to 12km. A study of $PM_{2.5}$ heath impact assessment with CMAQ by Jiang et al. (2018) found that model results at 12 km generally performed better and had substantially lower computational burden, compared to 4 km resolution. Here, we compared the global simulation (1 °×1 °) with the nested simulation (0.33 °×0.33 °) over China. Table 6 gives the statistics of $PM_{2.5}$, SO_2 and NO_2 simulated at different resolutions. The nested domain can effectively improve the simulating of city pollutants, especially $PM_{2.5}$, because high-resolution grid can provide better resolved emissions and meteorological fields in urban and rural areas. As shown in Table 6, the correlation coefficients of the three species in the nested simulations are significantly higher than in the global simulations. The RMSE of the nested results in most cities are reduced. For $PM_{2.5}$, the R for Guangzhou and Zhongshan increase by 0.2 and 0.25 respectively, and the R for Urumqi increases by 0.19. Moreover, the RMSE decreases over 9 cities. The improvements in SO_2 simulation is clear, with R increased over 8 cities and RMSE decreased over 9 cities. In particular, the simulation in NC, YRD and SCW improves significantly, with better representation of monthly variation and closer comparison to observations. For NO_2, the R is significantly increased in 9 cities and RMSE is decreased in 7 cities. The best performance is in Beijing with R increased from 0.48 to 0.68.

4. Conclusions

A global-nested aerosol and atmospheric chemistry model coupled into CAS-ESM is introduced in this study. The aim is to provide more precise information on climate effects and air pollution on both global and regional scales.

For the global simulation, the surface distribution of trace gases in the model agrees reasonably well with site observations, mostly within a factor of two. IAP-AACM underestimates CO over ocean mainly due to a higher oxidation loss and the underestimation of emissions over ocean. The model reproduces the annual distribution of O_3 well, with NMB ranging from -0.34 to 0.1 except Asia. Furthermore, the model represents seasonal variation of O_3 over most regions. The model shows an antifact of the ascending-in-spring and descending-in-summer pattern in the NH land. On one hand, the simulation bias is always associated with inaccurate meteorological conditions due to their impacts on photochemistry and intercontinental transportation. On the other hand, it's difficult for global models (with coarse resolution) to resolve the sharp gradient of underlying on the land. The simulation of NO_2 is consistent with site records with NMB within ±0.16. For SO_2, it shows a good agreement with observations except for an overestimation in eastern America and Europe. With a weak scavenging rate by deposition and oxidation, SO_2 in the model has a longer lifetime compared with other models and the burden (0.63 Tg S yr^{-1}) is at the high end of the range 0.2-0.69 Tg S yr^{-1}. The budgets of both carbonaceous aerosols and sulfate are similar to other models. At surface, IAP-AACM shows much closer results to observations for BC but more variable performance for secondary aerosols. In EA, simulations match records on sulfate (NMB=0.36). In NAmerica, simulations match records on nitrate and ammonium (NMB within ±0.5). It overestimates sulfate and ammonium (NMB=1.1 and 1.49 respectively) in Europe and overestimates sulfate (NMB=1.94) in America. The underestimation of OC is mainly due to the inadequate

formation of SOA and the underestimated emission for OC. Above the surface, IAP-AACM generally captures the seasonal and spatial features of O_3 and NO_2 VTC and AOD shown in the satellite products.

For the nested simulation, IAP-AACM shows a very similar annual distribution over EA and a more reasonable distribution on the boundary, compared with regional models from the MICS-Asia project. IAP-AACM shows a good agreement with observations from Chinese cities for spatio-temporal variation. The model compares well with observations for SO_2, with three-quarters cities' R ranging 0.6~0.89 and more than half of the cities' NMB within ±0.5. For NO_2, although more than half of the cities have a correlation above 0.5, there is an overestimation in NC, YRD and CC in summer. The model shows an over decomposition of HNO_3 in warm seasons due to the thermodynamic equilibrium module and heterogeneous mechanism. The underestimation of nitrate also relates to this problem. In most cities, IAP-AACM shows very good simulation skill for $PM_{2.5}$, with R near or above 0.7. For aerosol compositions, the simulation of BC shows better correlation coefficients (above 0.5) in all cities. The simulation of OC is lower than observations. The model results of sulfate and ammonium in NC are close to observations, but it underestimates the concentration in South China. The comparison between global (1°×1°) and nested (0.33°×0.33°) results indicates that the model reproduces the spatial variation of pollutants in the cities better at fine resolution, as large gradient of emissions between urban and nonurban areas and atmospheric circulations can be better captured by higher resolution grids.

In general, the model shows a favorable performance for trace gases and carbonaceous aerosols. Nevertheless, the simulation of secondary aerosols shows some weaknesses. To reduce uncertainties in the simulation of SNA, more work is needed to improve not only aerosol chemistry but also emission inventories. Moreover, the SOA module should be upgraded to incorporate a comprehensive scheme (e.g. Volatility Bias Set by Donahue et al. (2006)) and verified with observations.

Author contribution

Ying Wei did the reanalysis and writed the paper. Xueshun Chen, Huansheng Chen and Jie Li also contributed to the writing. Beasides, they and Zifa Wang, Wenyi Yang, Baozhu Ge are the model contributors. Huiyun Du, Jianqi Hao, Wei Wang, Jianjun Li, Yele Sun and Huili Huang provided data.

Acknowledgments:

Thanks to Jiangsu Environmental Monitoring Center and Wuhan Environmental Monitoring Center for their support with aerosol composition data of Nanjing and Wuhan respectively. We sincerely thank Prof. Hajime Akimoto at National Institute for Environmental Studies for his suggestion in improving this manuscript. We are particularly grateful to Prof. Oliver Wild at Lancaster University for his support with the HTAP model data and help in improving the language of this manuscript. This research is supported by the National Major Research High Performance Computing Program of China the National Major Research High Performance Computing Program of China (Grant NO. 2016YFB0200800), the Chinese Ministry of Science and Technology (Grant NO. 2017YFC0212402) and the Natural Science Foundation

of China (Grant NO. 41571130034; 91544227; 91744203; 41705108; 41620104008).

References

Akimoto, H.: Global air quality and pollution. Science, 302(5651), 1716, 2003.

Akritidis, D., Katragkou, E., Zanis, P.， et al. : A deep stratosphere-to-troposphere ozone transport event over Europe simulated in CAMS global and regional forecast systems: analysis and evaluation. Atmospheric Chemistry and Physics, 18, 15515–15534, doi: 10.5194/acp-18-15515-2018, 2018.

Andres, R. J., & Kasgnoc, A. D. :A time-averaged inventory of subaerial volcanic sulfur emissions, Journal of Geophysical Research Atmospheres, 103(D19), 25251-25261, doi: 10.1029/98JD02091 , 1998.

Athanasopoulou, E., Tombrou, M., Pandis, S. N., & Russell, A. G. : The role of sea-salt emissions and heterogeneous chemistry in the air quality of polluted coastal areas, Atmospheric Chemistry & Physics, 8(19), 5755-5769, doi: 10.5194/acp-8-5755-2008, 2008.

Austin, J.F., Follows, M.J. : The ozone record at Payerne: an assessment of the cross-tropopause flux. Atmospheric Envirnoment 25A, 1873-1880, doi: 10.1016/0960-1686(91)90270-H, 1991.

Badia, A., Jorba, O., Voulgarakis, A., Dabdub, D., Pérez Garc ápando, C., & Hilboll, A., et al. : Description and evaluation of the multiscale online nonhydrostatic atmosphere chemistry model (NMMB-MONARCH) version 1.0: gas-phase chemistry at global scale, Geoscientific Model Development, 10, 1-47, doi:10.5194/gmd-10-609-2017, 2017.

Boucher, O., D. Randall, P. Artaxo, C. Bretherton, G. Feingold, P. Forster, V.-M. Kerminen, Y. Kondo, H. Liao, U. Lohmann, P. Rasch, S.K. Satheesh, S. Sherwood, B. Stevens and X.Y. Zhang, 2013: Clouds and Aerosols. In: Climate Change 2013: The Physical Science Basis. Contribution of Working Group I to the Fifth Assessment Report of the Intergovernmental Panel on Climate Change [Stocker, T.F., D. Qin, G.-K. Plattner, M. Tignor, S.K. Allen, J. Boschung, A. Nauels, Y. Xia, V. Bex and P.M. Midgley (eds.)]. Cambridge University Press, Cambridge, United Kingdom and New York, NY, USA.

Burnett, R. T., Arden Pope, C., Ezzati, M., Olives, C., Lim, S. S., Mehta, S., Shin, H. H., Singh, G., Hubbell, B., Brauer, M., Ross, Anderson, H., Smith, K. R., Balmes, J. R., Bruce, N. G., Kan, H., Laden, F., Prüss-Ustün, A., Turner, M. C., Gapstur, S. M., Diver, W. R., and Cohen, A: An integrated risk function for estimating the global burden of disease attributable to ambient fine particulate matter exposure, Environ. Health Persp., 122, 397, https://doi.org/10.1289/ehp.1307049, 2014.

Calvert, J. G. : SO_2, NO and NO_2 oxidation mechanisms: atmospheric considerations, 1984.

Chen, C., Sun, Y. L., Xu, W. Q., Du, W., Zhou, L. B., & Han, T. T., et al. : Characteristics and sources of submicron aerosols above the urban canopy (260 m) in Beijing, china, during the 2014 APEC summit, Atmospheric Chemistry and Physics, 15, 12879–12895, doi: 10.5194/acp-15-12879-2015, 2015.

Chen, H. S., Wang, Z. F., Li, J., Tang, X., Ge, B. Z., & Wu, X. L., et al. : GNAQPMS-HG v1.0, a global nested atmospheric mercury transport model: model description, evaluation and application

to trans-boundary transport of Chinese anthropogenic emissions, Geoscientific Model Development, 8(5), 6949-6996, doi:10.5194/gmd-8-2857-2015, 2015.

Chen X. S., Wang, Z. F., Li, J. et al. : Simulation of particle number size distribution in Beijing in winter using NAQPMS+APM model. (in Chinese), 20 (6): 611−619, doi:10.3878/j.issn.1006-9585.2015.15095, 2015.

Chen, X. S., Wang, Z. F., Yu, F. Q., Pan, X. L., Li, J., & Ge, B. Z., et al. : Estimation of atmospheric aging time of black carbon particles in the polluted atmosphere over central-eastern china using microphysical process analysis in regional chemical transport model. Atmospheric Environment, 163(5): 44-56, doi: 10.1016/j.atmosenv.2017.05.016, 2017.

Cheng, Y., Zheng, G., Wei, C., Mu, Q., Zheng, B., & Wang, Z., et al. : Reactive nitrogen chemistry in aerosol water as a source of sulfate during haze events in china. Science Advances, 2(12), doi: 10.1126/sciadv.1601530, 2016.

Dai, Y. J., Zeng, X. B., Dickinson, R. E. , Baker, I. ,Bonan, G. B. & Bosilovich, M. G.: The common land model. Bulletin of the American Meteorological Society, 84(8), 1013-1023, 2015. doi:10.1175/BAMS-84-8-1013, 2015.

Dentener, F., Kinne, S., Bond, T., Boucher, O., Cofala, J., & Generoso, S., et al. : Emissions of primary aerosol and precursor gases in the years 2000 and 1750 prescribed data-sets for AeroCom. Atmospheric Chemistry & Physics, 6(12), 4321-4344, , doi:10.5194/acp-6-4321-2006, 2006.

Donahue N. M., Robinson A. L., Stanier C. O., et al. : Coupled partitioning, dilution, and chemical aging of semivolatile organics. Environmental Science & Technology, 40(8):2635-2643, doi: 10.1021/es052297c, 2006.

Emmons, L. K. , Walters, S. , Hess, P. G. , J.-F., L. , Pfister, G. G. , & Fillmore, D. , et al. : Description and evaluation of the Model for Ozone and Related Chemical Tracers, version 4 (MOZART-4). Geosci. Model Dev., 3, 43–67, doi: 10.5194/gmd-3-43-2010, 2010

Falk, S., & Sinnhuber, B. M. Polar boundary layer bromine explosion and ozone depletion events in the chemistry-climate model EMAC v2.52: implementation and evaluation of airsnow algorithm. Geoscientific Model Development, 11(3), 1-15, https://doi.org/10.5194/gmd-11-1115-2018, 2018.

Fiore，A. M., Dentener，F. J., Wild, O., et al. : Multimodel estimates of intercontinental source-receptor relationships for ozone pollution. JOURNAL OF GEOPHYSICAL RESEARCH, 114, D04301, doi:10.1029/2008JD010816, 2009, 2009.

Fu， T.-M., Cao, J. J., Zhang, X. Y., Lee, S. C., & Henze, D. K.: Carbonaceous aerosols in china: top-down constraints on primary sources and estimation of secondary contribution. Atmospheric Chemistry and Physics, 12(5), 2725-2746, doi:10.5194/acp-12-2725-2012, 2012.

Ganzeveld, L., Helmig, D., Fairall, C. W. , Hare, J. , & Pozzer, A. : Atmosphere-ocean ozone exchange: a global modeling study of biogeochemical, atmospheric, and waterside turbulence dependencies. Global Biogeochemical Cycles, 23(4), doi:10.1029/2008GB003301,2009.

Ge, B. Z., Wang, Z. F., Xu, X. B., Wu, J. B., Yu, X. L., and Li, J. Wet deposition of acidifying substances in different regions of China and the rest of East Asia: Modeling with updated NAQPMS. Environment Pollution, 187, 10-21, doi: 10.1016/j.envpol.2013.12.014, 2014.

Giorgi, F., Bi, X., & Qian, Y. : Indirect vs. direct effects of anthropogenic sulfate on the climate of East Asia as simulated with a regional coupled climate-chemistry/aerosol model. Climatic Change, 58(3), 345-376, 2003.

Granier, C., Lamarque, J. F., Mieville, A., Muller, J. F., and Olivier, J.: POET. : a database of surface emissions of ozone precursors, tech. report, available at: http://www.aero.jussieu.fr/projet/ACCENT/POET.php , 2005.

Han, Z., et al. MICS-Asia II: Model intercomparison and evaluation of ozone and relevant species, Atmos. Environ., 42, 3491 – 3509, doi:10.1016/j.atmosenv.2007.07.031, 2008.

Han, Z., Xie, Z., Wang, G., Zhang, R., & Tao, J. : Modeling organic aerosols over east china using a volatility basis-set approach with aging mechanism in a regional air quality model. Atmospheric Environment,124, 186-198, doi: 10.1016/j.atmosenv.2015.05.045, 2016.

Hardacre, C. , Wild, O. , & Emberson, L., et al. : An evaluation of ozone dry deposition in global scale chemistry climate models. Atmospheric Chemistry and Physics, 15, 6419–6436, doi:10.5194/acp-15-6419-2015, 2015.

He, H., Wang, Y., Ma, Q., Ma, J., Chu, B., & Ji, D., et al. : Corrigendum: mineral dust and nox promote the conversion of so2 to sulfate in heavy pollution days. Sci Rep, 4(1), 4172, doi: 10.1038/srep06092, 2014.

Horowitz, L. W., Walters, S., Mauzerall, D. L., Emmons, L. K., Rasch, P. J., Granier, C., Tie, X., Lamarque, J.-F., Schultz, M. G., Tyndall, G. S., Orlando, J. J., and Brasseur, G. P.: A global simulation of tropospheric ozone and related tracers: Description and evaluation of MOZART, version 2, J. Geophys. Res.-Atmos., 108, 4784, doi:10.1029/2002JD002853, 2003.

Houghton, J. E. T., Ding, Y. H., Griggs, J., Noguer, M., Pj, V. D. L., & Dai, X., et al. : IPCC 2001. Climate Change 2001: the scientific basis. Climate Change 2001: The Scientific Basis, 2001:227-239, 2001.

Huijnen, V., Williams, J., van Weele, M., van Noije, T., Krol, M., Dentener, F., and et al. : The global chemistry transport model TM5: description and evaluation of the tropospheric chemistry version 3.0, Geosci. Model Dev., 3, 445–473, doi:10.5194/gmd-3-445-2010, 2010.

Janssens-Maenhout, G., Crippa, M., Guizzardi, D., Dentener, F., Muntean, M., & Pouliot, G., et al. : HTAP_v2.2: a mosaic of regional and global emission grid maps for 2008 and 2010 to study hemispheric transport of air pollution. Atmospheric Chemistry & Physics, 15(8), 12867-12909, doi: 10.5194/acp-15-11411-2015, 2015.

Jiang, X. , & Yoo, E. H. : The importance of spatial resolutions of community multiscale air quality (CMAQ) models on health impact assessment. Science of The Total Environment, 627, 1528-1543, doi: 10.1016/j.scitotenv.2018.01.228, 2018.

Kaiser, J. C., Hendricks, J., Righi, M., Jöckel, P.,Tost, H.,Kandler, K., et al. : Global aerosol

modeling with MADE3 (v3.0) in EMAC (based on v2.53): model description and evaluation. Geoscientific Model Development Discussion. https://doi.org/10.5194/gmd-2018-185, 2018

Lamarque, J. F., Emmons, L. K., Hess, P. G., Kinnison, D. E., Tilmes, S., & Vitt, F., et al. : Cam-chem: description and evaluation of interactive atmospheric chemistry in the Community Earth System Model. Geoscientific Model Development, 5(2), 369-411, doi:10.5194/gmd-5-369-2012, 2012.

Lana, A., Bell, T. G., Simó, R., Vallina, S. M., Ballabrera-Poy, J., & Kettle, A. J., et al. : An updated climatology of surface dimethlysulfide concentrations and emission fluxes in the global ocean. Global Biogeochemical Cycles, 25(1), 3-25, doi: 10.1029/2010GB003850, 2011.

Lee, Y. H., & Adams, P. J. : Evaluation of aerosol distributions in the GISS-TOMAS global aerosol microphysics model with remote sensing observations. Atmospheric Chemistry & Physics, 10(5), 2129-2144, doi: 10.5194/acp-10-2129-2010, 2010.

Lee, Y. H., Lamarque, J. F., Flanner, M. G., Jiao, C., Shindell, D. T., & Berntsen, T., et al. : Evaluation of preindustrial to present-day black carbon and its albedo forcing from Atmospheric Chemistry and Climate Model Intercomparison Project (ACCMIP). Atmospheric Chemistry & Physics, 13(5), 2607-2634, doi: 10.5194/acp-13-6553-2013, 2013.

Lee, Y. H., Adams, P. J., & Shindell, D. T. : Evaluation of the global aerosol microphysical ModelE2-TOMAS model against satellite and ground-based observations. Geoscientific Model Development, 8(3), 631-667, doi:10.5194/gmd-8-631-2015, 2015.

Li, J., Z. Wang, et al. : Modeling study of ozone seasonal cycle in lower troposphere over east Asia. Journal of Geophysical Research-Atmospheres, 112(D22), doi: 10.1029/2006jd008209, 2007.

Li, J., Wang, Z., Wang, X., Yamaji, K., Takigawa, M., & Kanaya, Y., et al. : Impacts of aerosols on summertime tropospheric photolysis frequencies and photochemistry over central eastern china. Atmospheric Environment, 45(10), 1817-1829, doi: 10.1016/j.atmosenv.2011.01.016 , 2011.

Li, J., Z. Wang, et al. Mixing of Asian mineral dust with anthropogenic pollutants over East Asia: a model case study of a super-duststorm in March 2010. Atmospheric Chemistry and Physics, 12(16): 7591-7606, doi: 10.5194/acpd-12-2743-2012, 2012.

Li, J., Yang, W., Wang, Z., Chen, H., Hu, B., et al. Modeling study of surface ozone source-receptor relationships in East Asia. Atmospheric Research, 167, 77-88, doi: 10.1016/j.atmosres.2015.07.010, 2016.

Li, J., Chen, X., Wang, Z., Du, H., Yang, W., & Sun, Y., et al. : Radiative and heterogeneous chemical effects of aerosols on ozone and inorganic aerosols over East Asia, Science of the Total Environment, 622, 1327-1342, https://doi.org/10.1016/j.scitotenv.2017.12.041, 2018.

Li, Y., & Xu, Y..: Uptake and storage of anthropogenic CO_2 in the pacific ocean estimated using two modeling approaches. Advances in Atmospheric Sciences, 29(4), 795-809, 2012. doi: 10.1007/s00376-012-1170-4, 2012.

Lin, J., An, J., Yu, Q., Yong, C., Ying, L., & Tang, Y., et al. Local and distant source contributions to secondary organic aerosol in the Beijing urban area in summer. Atmospheric

Environment, 124, 176-185, doi: 10.1016/j.atmosenv.2015.08.098, 2016.

Liu, H., Lin, P., Yu, Y. Q., & Zhang, X. : The baseline evaluation of LASG/IAP climate system ocean model (LICOM) version 2. Journal of Meteorological Research, 26(3), 318-329, 2012.

Liu, X., Penner, J. E., & Herzog, M. : Global modeling of aerosol dynamics: model description, evaluation, and interactions between sulfate and nonsulfate aerosols, Journal of Geophysical Research Atmospheres, 110(D18), doi: 10.1029/2004JD005674, 2005

Lu, Z, Zhang, Q, & Streets, D. G.: Sulfur dioxide and primary carbonaceous aerosol emissions in China and India, 1996–2010. Atmospheric Chemistry and Physics, 11(18), 9839-9864, doi: 10.5194/acp-11-9839-2011, 2011.

Luo, G., & WANG Z. F. A Global Environmental Atmospheric Transport Model (GEATM): Model Description and Validation, Atmospheric Science, 30(3), 504-518, doi: 10.1016/S1003-6326(06)60040-X, 2006.

Mann, G. W., Carslaw, K. S., Spracklen, D. V., Ridley, D. A., Manktelow, P. T., & Chipperfield, M. P., et al. : Description and evaluation of GLOMAP-mode: a modal global aerosol microphysics model for the UKCA composition-climate model, Geoscientific Model Development, 3(2), 519-551, doi: 10.5194/gmd-3-519-2010, 2010.

Mathur, R., & Dennis, R. L. : Seasonal and annual modeling of reduced nitrogen compounds over the eastern United States: Emissions, ambient levels, and deposition amounts, Journal of Geophysical Research Atmospheres, 108(D15), 22-1 – 22-15, 2003.

Mebust, M. R., Eder, B. K., Binkowski, F. S., & Roselle, S. J. : Models-3 Community Multiscale Air Quality (CMAQ) model aerosol component 2. model evaluation. Journal of Geophysical Research Atmospheres, 108(D6), doi: 10.1029/2001JD001410, 2003.

Monks, P. S. A review of the observations and origins of the spring ozone maximum. Atmospheric Environment, 34(21), 3545-3561, doi: 10.1016/s1352-2310(00)00129-1, 2000.

Munzert, K. , Reiter, R. , Kanter, H. J. , & K. Pötzl. : Effect of Stratospheric Intrusions on the Tropospheric Ozone. In Proceedings of the Quad. Ozone Symposium, Halkidiki, Reidel, Dordecht, pp. 735-739, doi: 10.1007/978-94-009-5313-0_144, 1985.

Myhre, G., D. Shindell, F.-M. Bréon, W. Collins, J. Fuglestvedt, J. Huang, D. Koch, J.-F. Lamarque, D. Lee, B. Mendoza, T. Nakajima, A. Robock, G. Stephens, T. Takemura and H. Zhang, 2013: Anthropogenic and Natural Radiative Forcing. In: Climate Change 2013: The Physical Science Basis. Contribution of Working Group I to the Fifth Assessment Report of the Intergovernmental Panel on Climate Change [Stocker, T.F., D. Qin, G.-K. Plattner, M. Tignor, S.K. Allen, J. Boschung, A. Nauels, Y. Xia, V. Bex and P.M. Midgley (eds.)]. Cambridge University Press, Cambridge, United Kingdom and New York, NY, USA.

Naik, V., Voulgarakis, A., Fiore, A. M., Horowitz, L. W., Lamarque, J.-F., Lin, M., Prather, M. J., Young, P. J., Bergmann, D., Cameron-Smith, P. J., Cionni, I., Collins, W. J., Dalsøren, S. B., Doherty, R., Eyring, V., Faluvegi, G., Folberth, G. A., Josse, B., Lee, Y. H., MacKenzie, I. A., Nagashima, T., van Noije, T. P. C., Plummer, D. A., Righi, M., Rumbold, S. T., Skeie, R., Shindell, D. T., Stevenson, D. S., Strode, S., Sudo, K., Szopa, S., and Zeng, G.: Preindustrial

to present-day changes in tropospheric hydroxyl radical and methane lifetime from the Atmospheric Chemistry and Climate Model Intercomparison Project (ACCMIP), Atmos. Chem. Phys., 13, 5277–5298, doi:10.5194/acp-13-5277-2013, 2013.

Nenes, A., S. Pandis, et al. : ISORROPIA: A New Thermodynamic Equilibrium Model for Multiphase Multicomponent Inorganic Aerosols, Aquatic Geochemistry, 4(1): 123-152, doi: 10.1023/a:1009604003981, 1998.

Nenes, A., S. N. Pandis, et al. : Continued development and testing of a new thermodynamic aerosol module for urban and regional air quality models, Atmospheric Environment, 33(10): 1553-1560, doi: 10.1016/s1352-2310(98)00352-5, 1999.

Penner, J. E., Chuang, C. C. and Grant, K. : Climate forcing by carbonaceous and sulfate aerosols, Climate Dynamics, 14(12), 839-851, doi: 10.1007/s003820050259, 1998.

Penner, J. E., Andreae, M., Annegarn, H., et al. : climate change 2001: the scientific basis, contribution of working group I to the third assessment report of the IPCC, 2001.

Pope III, C. A., Burnett, R. T., Turner, M. C., Cohen, A., Krewski, D., Jerrett, M. et al.: Lung cancer and cardiovascular disease mortality associated with ambient air pollution and cigarette smoke: shape of the exposure–response relationships, Environ. Health Persp., 119, 1616, https://doi.org/10.1289/ehp.1103639, 2011.

Powell, H., Krall, J. R., Wang, Y., Bell, M. L., and Peng, R. D.: Ambient coarse particulate matter and hospital admissions in the Medicare Cohort Air Pollution Study, 1999–2010, Environ. Health Persp., 123, 1152, https://doi.org/10.1289/ehp.1408720, 2015.

Price, C., J. Penner, & M. Prather. : NOx, from lightning: 1. global distribution based on lightning physics. Journal of Geophysical Research: Atmospheres, 102(D5), 5929-5941, 1997.

Randerson, J. T., G. R. vander Werf, L. Giglio, G. J. Collatz, and P. S. Kasibhatla. : Global Fire Emissions Database, Version 4, (GFEDv4). ORNL DAAC, Oak Ridge, Tennessee, USA. https://doi.org/10.3334/ORNLDAAC/1293, 2015.

Richardson, M. I., Toigo, A. D. and Newman, C. E: Planet WRF: A General Purpose, Local to Global Numerical Model for Planetary Atmosphere and Climate Dynamics, Journal of Geophysical Research, 112, E09001, doi:10.1029/2006JE002825, 2007.

Saxena, P., and Seigneur, C.: On the oxidation of SO_2 to sulfate in atmospheric aerosols. Atmospheric Environment, 21(4), 807-812, 1987.

Schaap, M., Otjes, R. P., and Weijers, E. P. : Illustrating the benefit of using hourly monitoring data on secondary inorganic aerosol and its precursors for model evaluation. Atmospheric Chemistry & Physics, 11(21), 11041-11053, doi: 10.5194/acpd-10-12341-2010, 2011.

Shindell, D. T., G. Faluvegi, et al. : Multimodel simulations of carbon monoxide: Comparison with observations and projected near-future changes, Journal of Geophysical Research-Atmospheres111 (D19), doi: 10.1029/2006JD007100, 2006.

Shindell, D. T., Lamarque, J. F., Schulz, M., Flanner, M., Jiao, C., & Chin, M., et al. Radiative forcing in the ACCMIP historical and future climate simulations, Atmospheric Chemistry &

Physics, 13(3), 2939-2974, doi:10.5194/acp-13-2939-2013, 2013.

Simpson, W. R., von Glasow, R., Riedel, K., Anderson, P., Ariya, P., Bottenheim, J., Burrows, J., Carpenter, L. J., Frieß, U., Goodsite, M. E., Heard, D., Hutterli, M., Jacobi, H.-W., Kaleschke, L., Neff, B., Plane, J., Platt, U., Richter, A., Roscoe, H., Sander, R., Shepson, P., Sodeau, J., Steffen, A., Wagner, T., and Wolff, E.: Halogens and their role in polar boundary-layer ozone depletion, Atmos. Chem. Phys., 7, 4375–4418, doi:10.5194/acp-7-4375-2007, 2007.

Sindelarova, K., Granier, C., Bouarar, I., Guenther, A., Tilmes, S., Stavrakou, T., Müller, J.-F., Kuhn, U., Stefani, P., and Knorr, W. : Global dataset of biogenic VOC emissions calculated by the MEGAN model over the last 30 years, Atmospheric Chemistry & Physics, 14(17), 10725-10788, doi:10.5194/acpd-14-10725-2014, 2014.

Søvde, O. A., Prather, M. J., Isaksen, I. S. A., & Berntsen, T. K. : The chemical transport model OSLO CTM3. Geoscientific Model Development, 5(6), 1441-1469, doi: doi:10.5194/gmd-5-1441-2012, 2012.

Stevens, R. G., Pierce, J. R., Brock, C. A., Reed, M. K., Crawford, J. H., & Holloway, J. S., et al. : Nucleation and growth of sulfate aerosol in coal-fired power plant plumes: sensitivity to background aerosol and meteorology. Atmospheric Chemistry & Physics, 12(1), 189-206, doi: 10.5194/acp-12-189-2012, 2012.

Stockwell, W. R., Kirchner, F., Kuhn, M., & Seefeld, S. : A new mechanism for regional atmospheric chemistry modeling, Journal of Geophysical Research Atmospheres, 102(D22), 25847-25879, doi: 10.1029/97JD00849, 1997.

Strader, R., F. Lurmann, et al. : Evaluation of secondary organic aerosol formation in winter, Atmospheric Environment, 33(29): 4849-4863, doi: 10.1016/s1352-2310(99)00310-6 , 1999.

Sudo, K., Takahashi, M., Kurokawa, J. I., & Akimoto, H. : Chaser: A global chemical model of the troposphere 1. Model description. Journal of Geophysical Research Atmospheres, 107(D17), ACH-1-ACH 7-20, 10.1029/2001jd001113, 2002.

Su, T., Xue, F., & Zhang, H. : Simulating the intraseasonal variation of the East Asian summer monsoon by IAP AGCM 4.0, Advances in Atmospheric Sciences, 31(3), 570-580, 2014.

Tang Y., Dong, W., Li, L., Xue, W., Wang, B.. : CPL7 and its application prospect in the Earth system models of China, Advances in Earth Science, 30(5):620-625, 2015. (in Chinese)

Textor, C., Schulz, M., Guibert, S., Kinne, S., Balkanski, Y., & Bauer, S., et al. : Analysis and quantification of the diversities of aerosol life cycles within AEROCOM, Atmospheric Chemistry & Physics, 6, 1777-1813, doi: 10.5194/acpd-5-8331-2005, 2006.

Tie, X., Zhang, Q., He, H., Cao, J., Han, S., & Gao, Y., et al. : A budget analysis of the formation of haze in Beijing. Atmospheric Environment, 100, 25-36, 2015.

Tie X, Huang R J, Cao J, et al. Severe Pollution in China Amplified by Atmospheric Moisture, Scientific Reports, 7(1):15760, 2017.

Tsigaridis, K., Krol, M., Dentener, F. J., & Balkanski, Y. : Change in global aerosol composition since preindustrial times, Atmospheric Chemistry & Physics, 6(12), 5143-5162, 2006.

Tsigaridis, K., Daskalakis, N., Kanakidou, M., Adams, P. J., Artaxo, P., & Bahadur, R., et al. : The AEROCOM evaluation and intercomparison of organic aerosol in global models, Atmospheric Chemistry & Physics, 14(5), 6027-6161, 2014.

Tuccella, P., Curci, G., Visconti, G., Bessagnet, B., Menut, L., & Park, R. J. : Modeling of gas and aerosol with wrf/chem over europe: evaluation and sensitivity study, Journal of Geophysical Research Atmospheres, 117(D3), doi: 10.1029/2011JD016302, 2012.

Wang, L. T., Wei, Z., Yang, J., Zhang, Y., Zhang, F. F., & Su, J., et al. : The 2013 severe haze over the southern Hebei, China: Model evaluation, source apportionment, and policy implications, Atmospheric Chemistry & Physics, 14(6), 3151-3173, doi: 10.5194/acp-14-3151-2014, 2014.

Wang, Y. X., Mcelroy, M. B., Jacob, D. J., & Yantosca, R. M. : A nested grid formulation for chemical transport over Asia: Applications to CO, Journal of Geophysical Research, 109(D22), 2285-2311, 2008.

Wang, Y., Li, L., Chen, C., Huang, C., Huang, H., & Feng, J., et al. : Source apportionment of fine particulate matter during autumn haze episodes in Shanghai, China, Journal of Geophysical Research Atmospheres, 119(4), 1903–1914, DOI: 10.1002/2013JD019630, 2014.

Wang, Z. F., Ueda, H., & Huang, M. : A deflation module for use in modeling long-range transport of yellow sand over East Asia, Journal of Geophysical Research Atmospheres, 105(D22), 26947-26959, doi: 10.1029/2000JD900370, 2000.

Wang, Z., Li, J., Wang, X., Pochanart, P., & Akimoto, H. Modeling of regional high ozone episode observed at two mountain sites (MT. Tai and Huang) in East China. Journal of Atmospheric Chemistry, 55(3), 253-272, doi: 10.1007/s10874-006-9038-6, 2006a.

Wang, Z. F., Xie, F. Y., Wang X. Q., An J. L., Zhu, J. : Development and Application of Nested Air Quality Prediction Modeling System, Chinese Journal of Atmospheric Sciences, 30(5),778-790, 2006b. (in Chinese)

Wang, Z. F., Xie, F., Sakurai, T., Ueda, H., Han, Z., & Carmichael, G. R., et al. : Mics-Asia II: model inter-comparison and evaluation of acid deposition, Atmospheric Environment, 42(15), 3528-3542, 2008.

Wei, Y., Li, J., Wang, Z. F., Chen, H. S., Wu, Q. Z., et al. Trends of surface $PM_{2.5}$ over Beijing–Tianjin–Hebei in 2013–2015 and their causes: emission controls VS. meteorological conditions, Atmospheric and Oceanic Science Letters, 10(4), 276-283, doi: 10.1080/16742834.2017.1315631, 2017.

Werf, G. R. V. D., Randerson, J. T. , Giglio, L. , Leeuwen, T. T. V. , Chen, Y. , & Rogers, B. M. , et al. : Global fire emissions estimates during 1997–2016. Earth System Science Data, 9(2), 697-720. https://doi.org/10.5194/essd-9-697-2017, 2017.

Wesely, M. L. : Parameterization of surface resistances to gaseous dry deposition in regional-scale numerical models, Atmospheric Environment, 23(6), 1293-1304, doi:

10.1016/0004-6981(89)90153-4, 1989.

Wu, Q. Z., Z. F. Wang, et al. A numerical study of contributions to air pollution in Beijing during CAREBeijing-2006, Atmospheric Chemistry and Physics, 11(12), 5997-6011, 2011.

Xu, R. T., Tian, H. Q., Pan, S. F., Prior, S. A., Feng, Y. C., & Batchelor, W. D., et al.: Global ammonia emissions from synthetic nitrogen fertilizer applications in agricultural systems: Empirical and process-based estimates and uncertainty. Global Change Biology, 25, 314-325, doi: 10.1111/gcb.14499, 2019.

Yan, X. Y., Ohara, T., & Akimoto, H. : Statistical modeling of global soil NOx emissions. Global Biogeochemical Cycles, 19(3), 2005.

Yang, W. Y., Li, J., Wang, M., Sun Y. L., Wang, Z. F. : A Case Study of Investigating Secondary Organic Aerosol Formation Pathways in Beijing using an Observation-based SOA Box Model, Aerosol and Air Quality Research, 18: 1606–1616, doi: 10.4209/aaqr.2017.10.0415, 2018.

Young, P. J., Naik, V., Fiore, A. M., et al. 2018 Tropospheric Ozone Assessment Report: Assessment of global-scale model performance for global and regional ozone distributions, variability, and trends. Elem Sci Anth, 6: 10. DOI: https://doi.org/10.1525/elementa.265,2018.

Yu, F. and Luo, G.: Simulation of particle size distribution with a global aerosol model: contribution of nucleation to aerosol and CCN number concentrations, Atmos. Chem. Phys., 9, 7691– 7710, doi:10.5194/acp-9-7691-2009, 2009.

Zaveri, R. and L. Peters: A new lumped structure photochemical mechanism for large-scale application, Journal of Geophysical Research-Atmospheres, 104(D23), doi: 10.1029/1999JD900876, 1999.

Zhang, L. M., Brook, J. R., & Vet, R. : A revised parameterization for gaseous dry deposition in air-quality models, Atmos.chem.phys, 3(2), 2067-2082, doi: 10.5194/acp-3-2067-2003, 2003.

Zhang, Q., Quan, J., Tie, X., Li, X., Liu, Q., & Gao, Y., et al. : Effects of meteorology and secondary particle formation on visibility during heavy haze events in Beijing, China, Science of the Total Environment, 502, 578-584, 2015.

Zhang, X. Y., Wang, Y. Q., Zhang, X. C., Guo, W., & Gong, S. L. : Carbonaceous aerosol composition over various regions of china during 2006, Journal of Geophysical Research, 113(D14), doi: 10.1029/2007JD009525, 2008.

Zhao, B., Wang, S., Donahue, N. M., Jathar, S. H., & Robinson, A. L. : Quantifying the effect of organic aerosol aging and intermediate-volatility emissions on regional-scale aerosol pollution in china. Scientific Reports, 6, doi: 10.1038/srep28815, 2016.

Zheng, B., Zhang, Q., Zhang, Y., He, K. B., Wang, K., & Zheng, G. J., et al. : Heterogeneous chemistry: a mechanism missing in current models to explain secondary inorganic aerosol formation during the January 2013 haze episode in North China, Atmospheric Chemistry & Physics, 14(15), 2031-2049, doi:10.5194/acp-15-2031-2015, 2015.

Zheng, B., Tong, D., Li, M., Liu, F., Hong, C. P., Geng, G. N., et al. : Trends in China's

anthropogenic emissions since 2010 as the consequence of clean air actions, Atmospheric Chemistry & Physics, 18(19), 14095-14111. https://doi.org/10.5194/acp-18-14095-2018, 2018.

Zhu, J., Zeng, X., Zhang, M., Dai, Y., Ji, D., & Li, F., et al. : Evaluation of the new dynamic global vegetation model in CAS-ESM, Advances in Atmospheric Sciences, 35(6), 659-670, 2018.

Figures

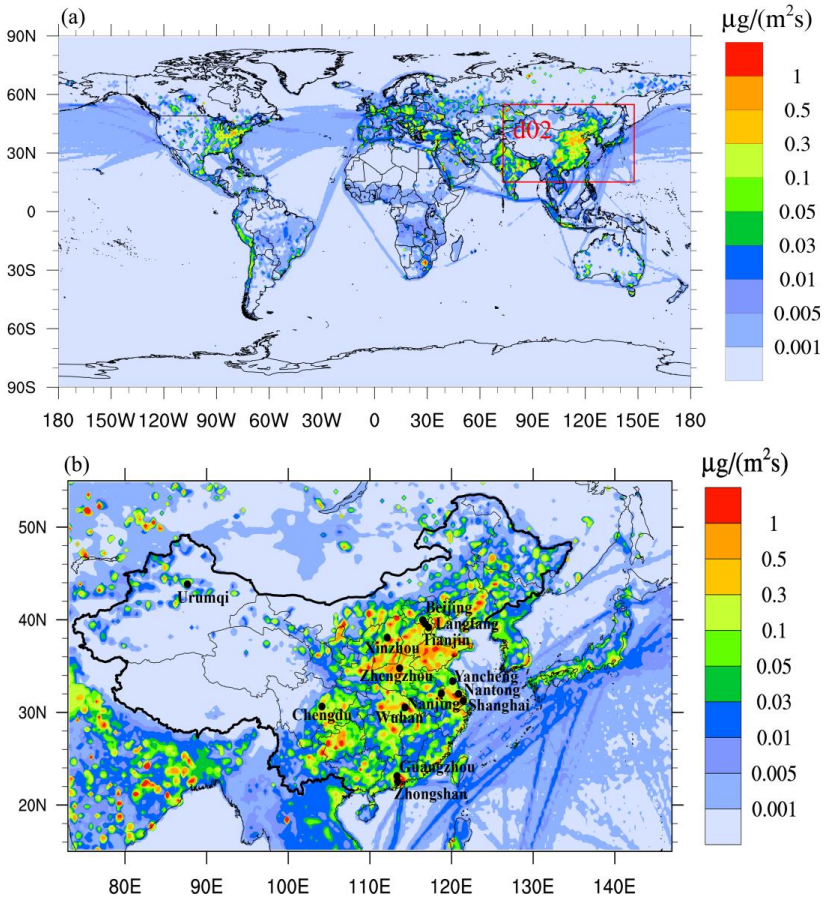

1165 Fig. 1. The simulation domain with total SO_2 emission (μg m^{-2} s^{-1}). (a) domain 1; (b) domain 2, black circles are locations of the city sites in China.

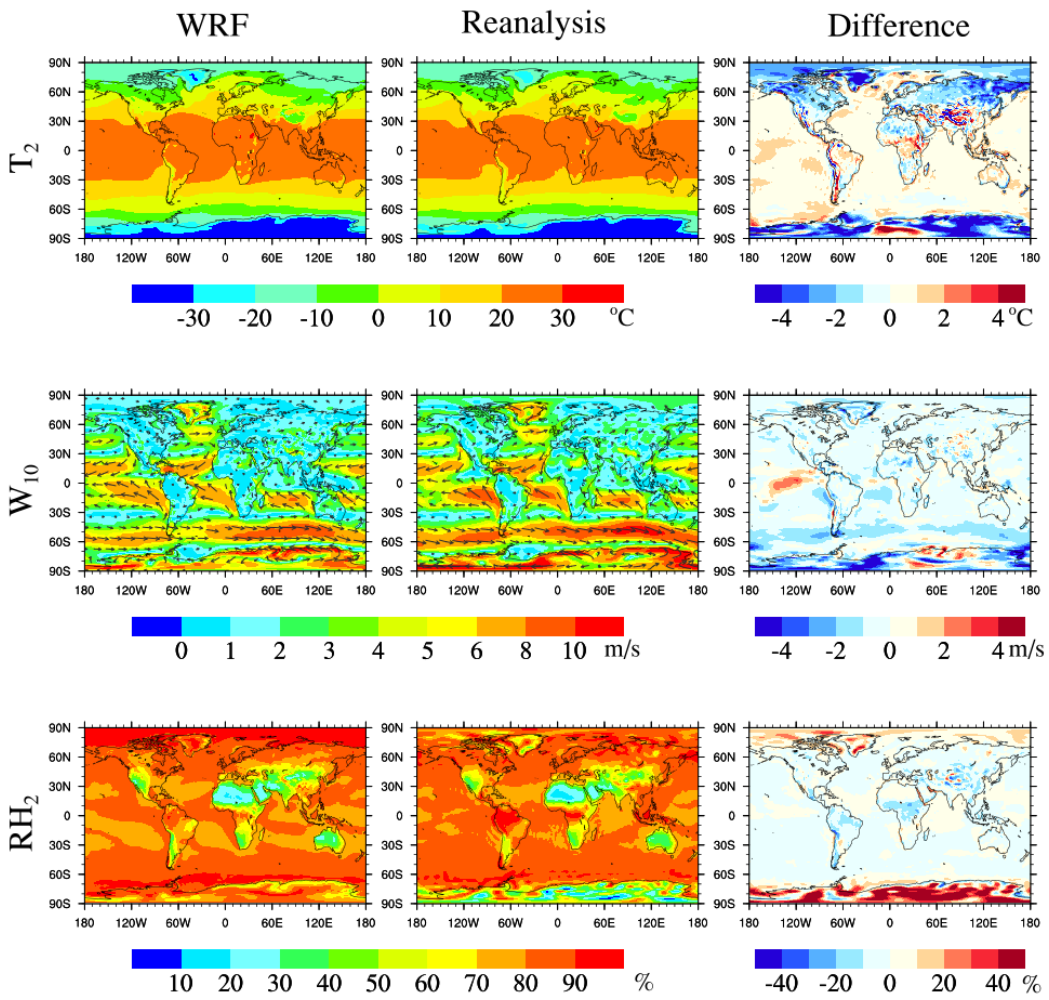

Fig. 2. Comparison of annual meteorological fields. The left column is WRF simulation, the middle column is reanalysis data, and the right column is the difference between simulation and reanalysis (WRF-Reanalysis). The reanalysis data is NCEP Reanalysis1.

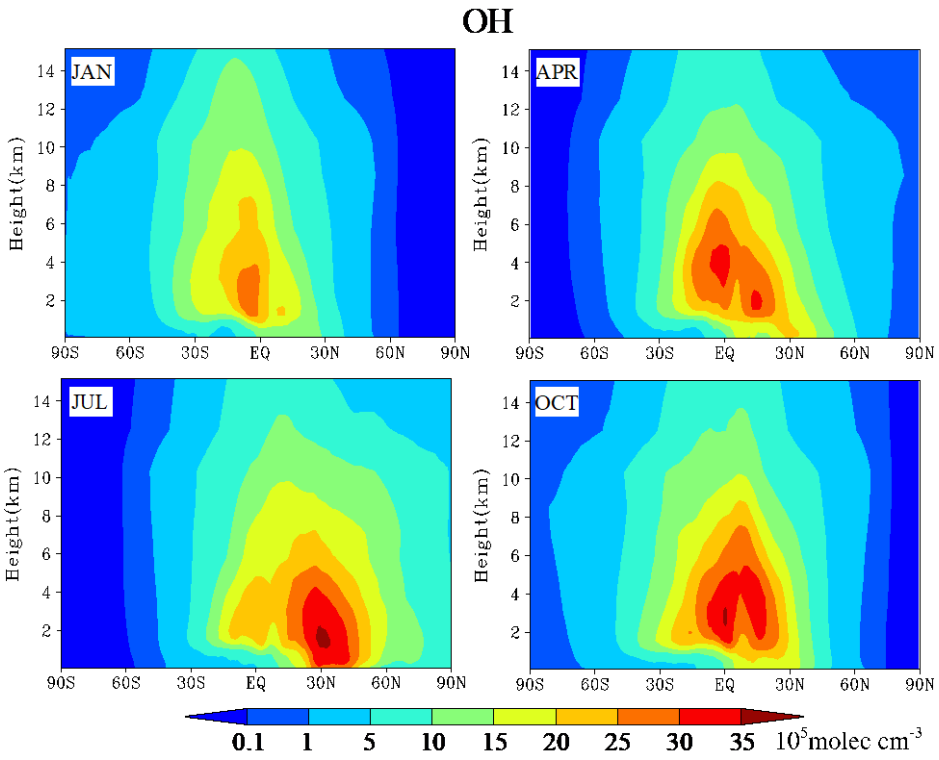

Fig. 3 Zonal monthly mean concentration of OH in the troposphere for January, April, July and October by the IAP-AACM. The unit is 10^5 molecule cm^{-3}.

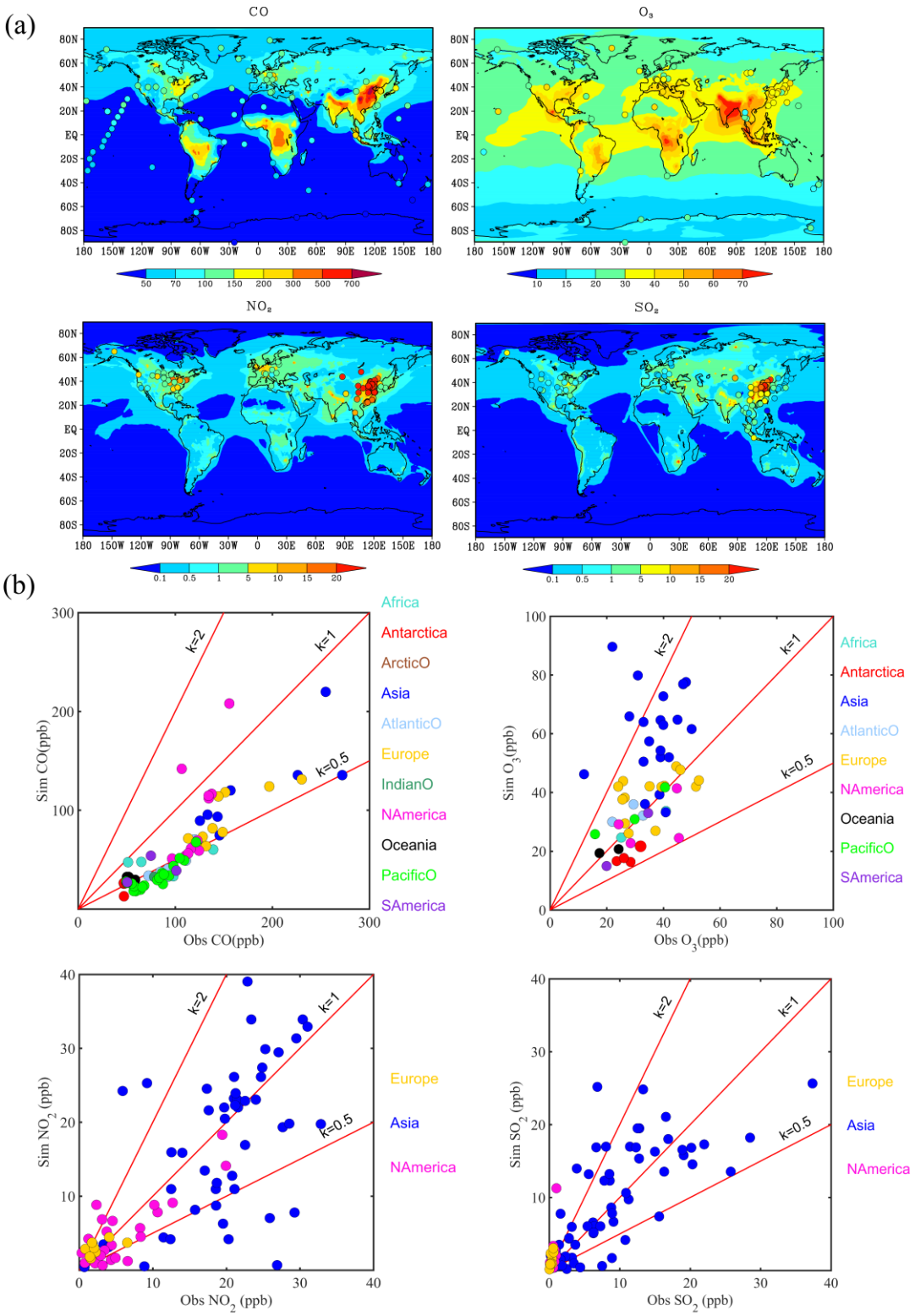

Fig. 4. Annual mean concentration (ppb) of the surface layer in IAP-AACM compared with observations. (a) The circles represent site observations. The first row is CO and O_3, the bottom row is NO_2 and SO_2. (b) Scatter plots in Africa, Antarctica, Arctic Ocean (ArcticO), Asia, Atlantic Ocean (AtlanticO), Europe, Indian Ocean (IndianO), North America (NAmerica), South America (SAmerica), Oceania and Pacific Ocean

(PacificO). The abscissa shows the observation and the ordinate shows the simulation. The color of the points represents different regions.

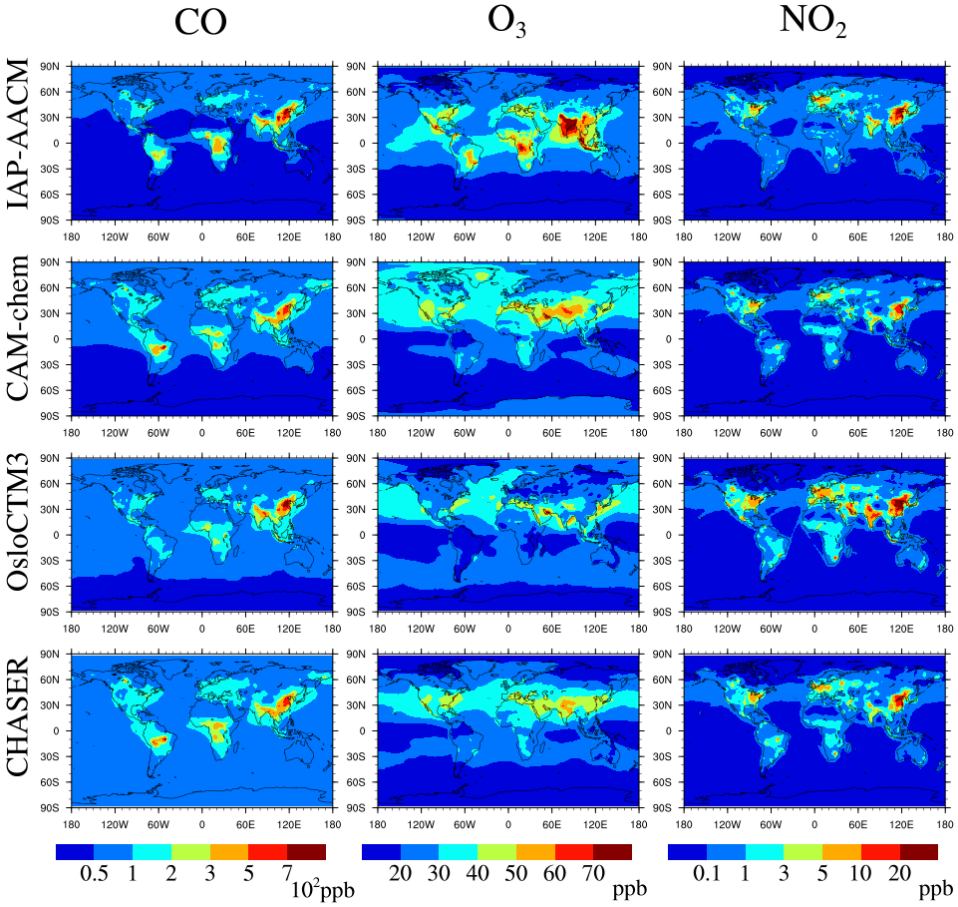

Fig. 5. Annual mean surface distributions (ppb) from IAP-AACM compared with HTAP models. Rows from top to bottom represent IAP-AACM, CAM-Chem, OsloCTM3 and CHASER respectively. The left column displays CO, the middle column displays O_3 and the right column is NO_2.

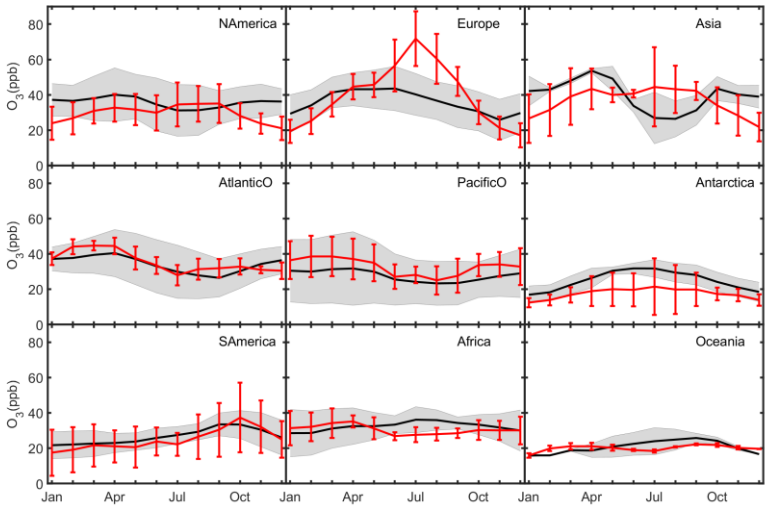

Fig. 6. Mean seasonal variation of O_3 (ppb) over NAmerica, Europe, Asia, AtlanticO, PacificO, Antarctica, SAmerica, Africa and Oceania sites. Black lines and red lines represent the average of observations and simulations respectively. Gray shaded areas

and red vertical bars show 1 standard deviation over the sites for observations and for model results respectively.

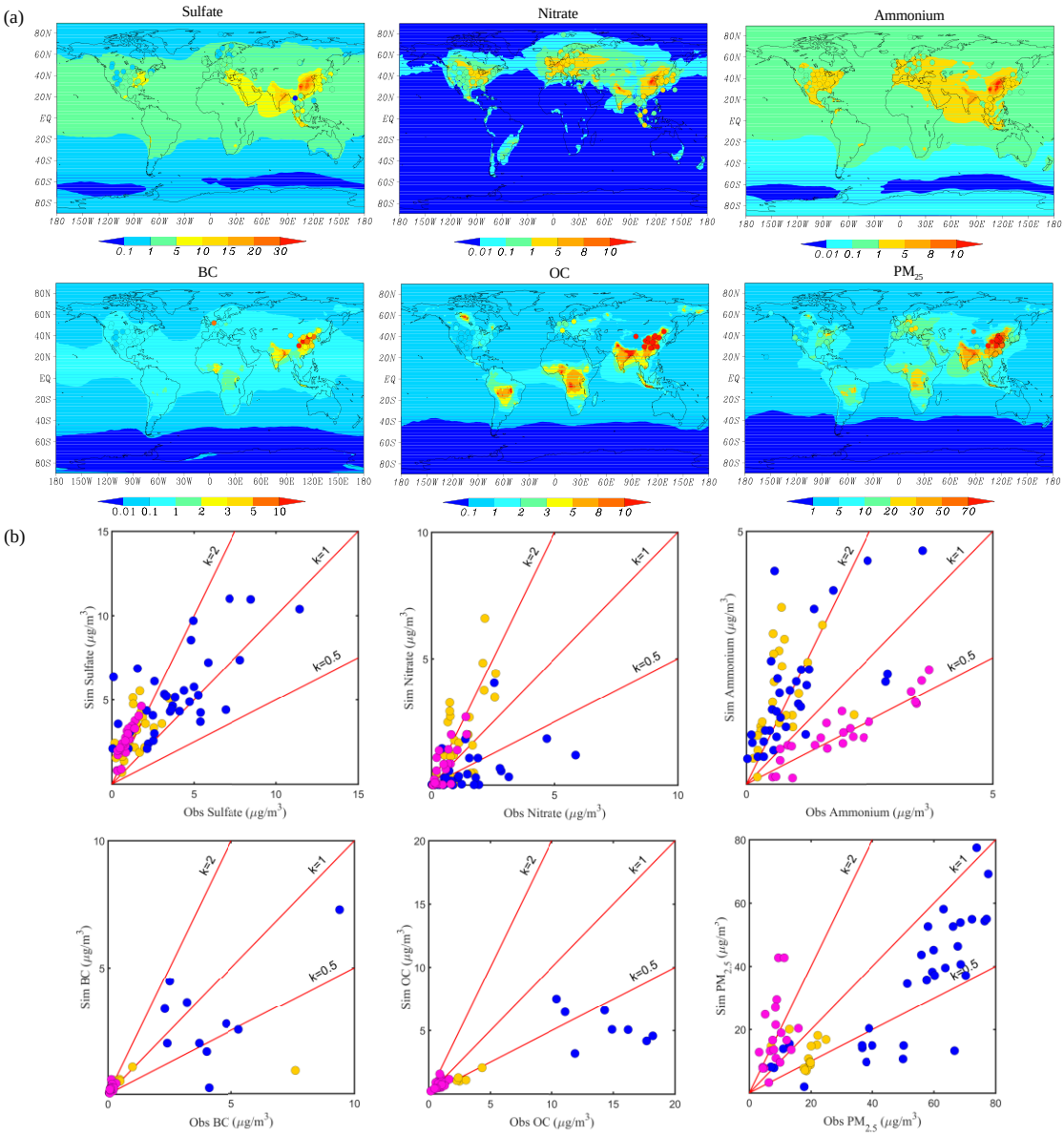

Fig. 7. (a) The same as Fig. 4, except the species are sulfate, nitrate, ammonium, BC, OC, and $PM_{2.5}$ and the unit is μg m^{-3}. The top row is sulfate, nitrate and ammonium, the bottom row is BC, OC and $PM_{2.5}$. (b) Scatter plot of annual mean concentration. The order of the subplot is in accordance with Fig. 7(a). Solid circles in blue, yellow and magenta represent Asia, Europe and NAmerica, respectively.

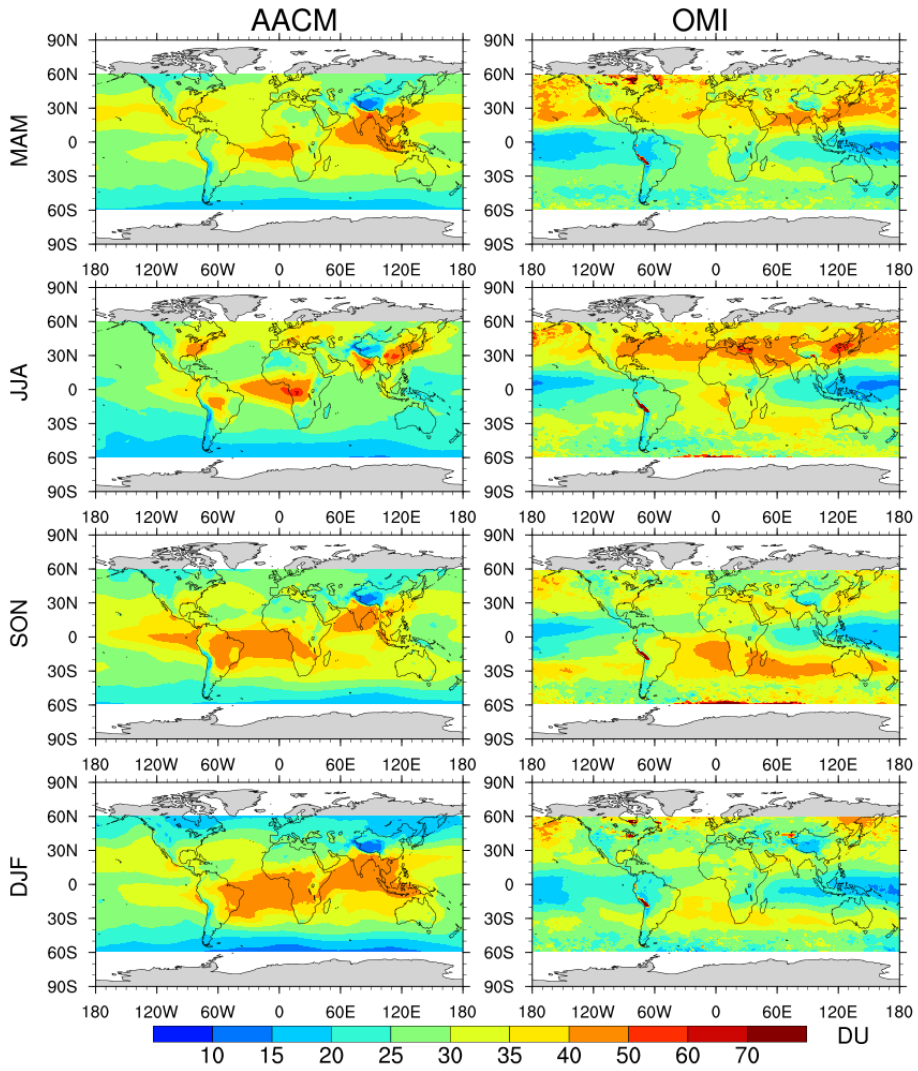

Fig. 8. Seasonal mean column concentration of O_3 from IAP-AACM (left column) and OMI (right column). Seasons are defined as March-April-May (MAM), June-July-August (JJA), and September-October-November (SON), and December-January-February (DJF). The unit is DU.

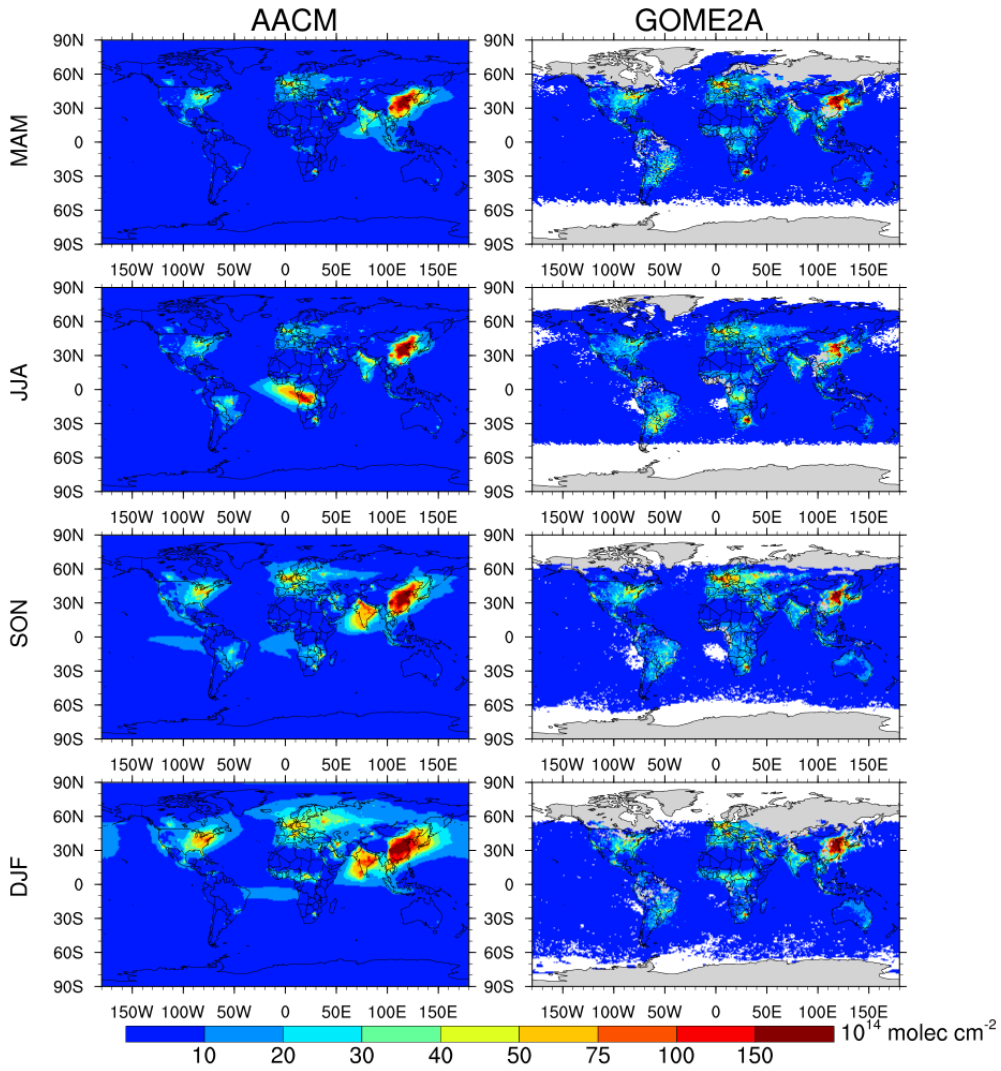

Fig. 9. Seasonal mean column concentration of NO_2 from IAP-AACM (left column) and GOME-2A (right column). The unit is 10^{14} molecule cm^{-2}.

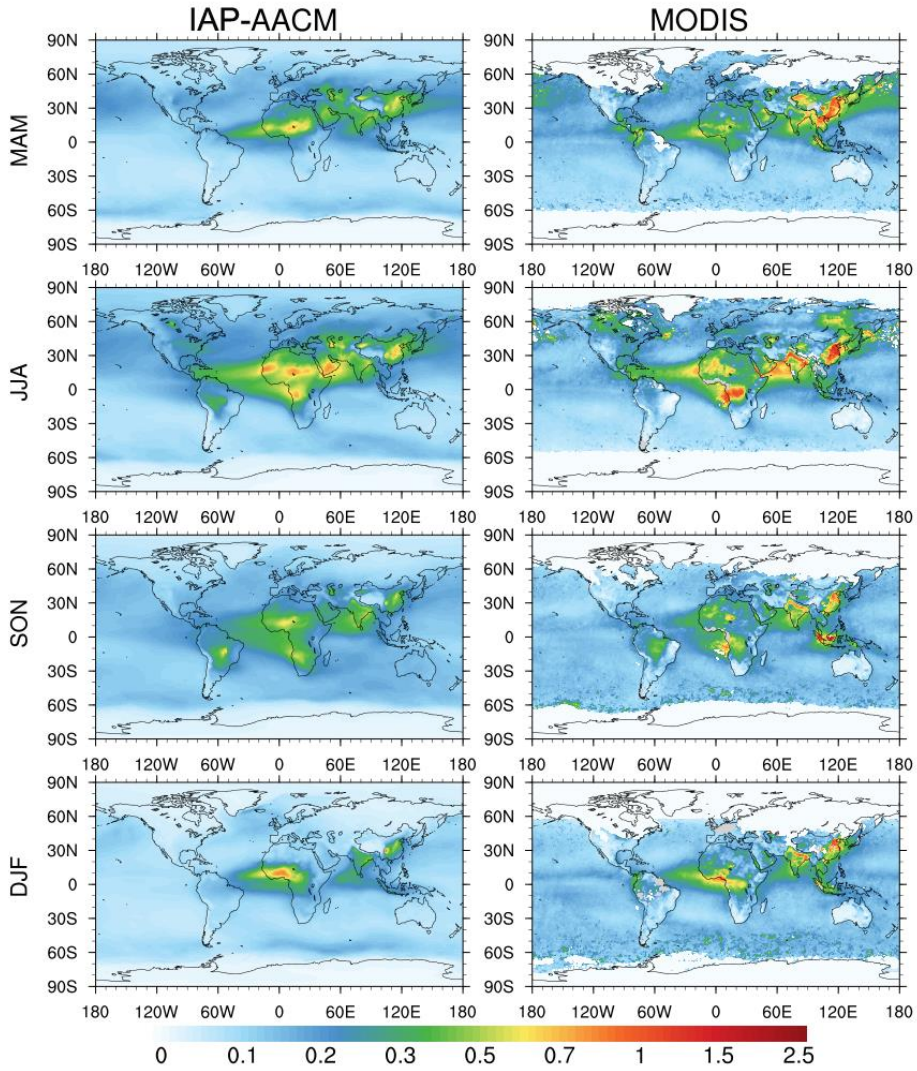

Fig. 10. Seasonal mean AOD from IAP-AACM (left column) and MODIS (right column).

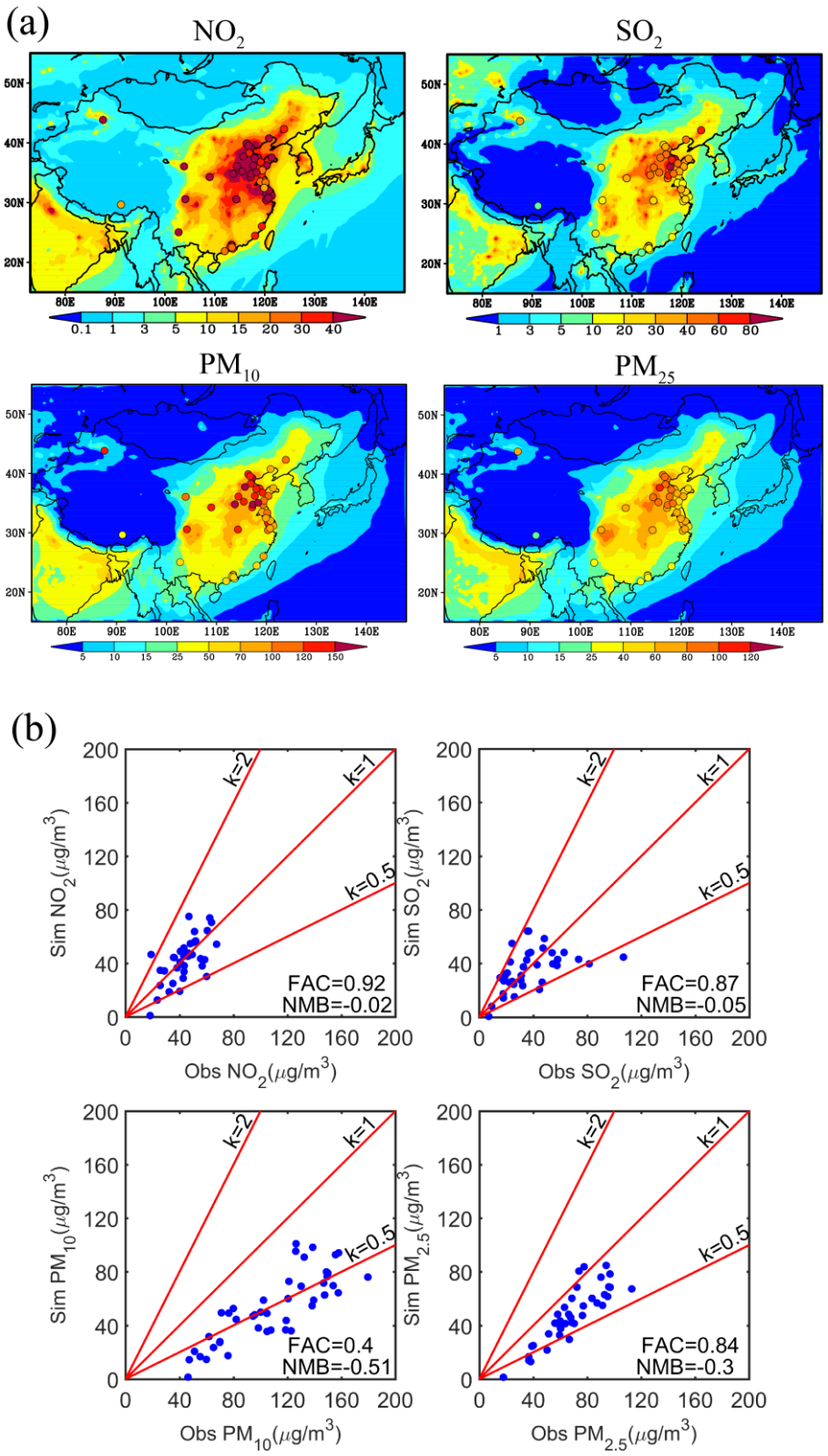

Fig. 11. (a) Surface annual mean concentration (μg m^{-3}) of the nested domain. The circles represent sites observations. The top row is NO_2 and SO_2, the bottom row is PM_{10} and $PM_{2.5}$. (b) Scatter plots of annual mean concentrations (μg m^{-3}) in nested domain. The order of the subplot is in accordance with Fig. 11(a). The abscissa shows the observation and the ordinate shows the simulation.

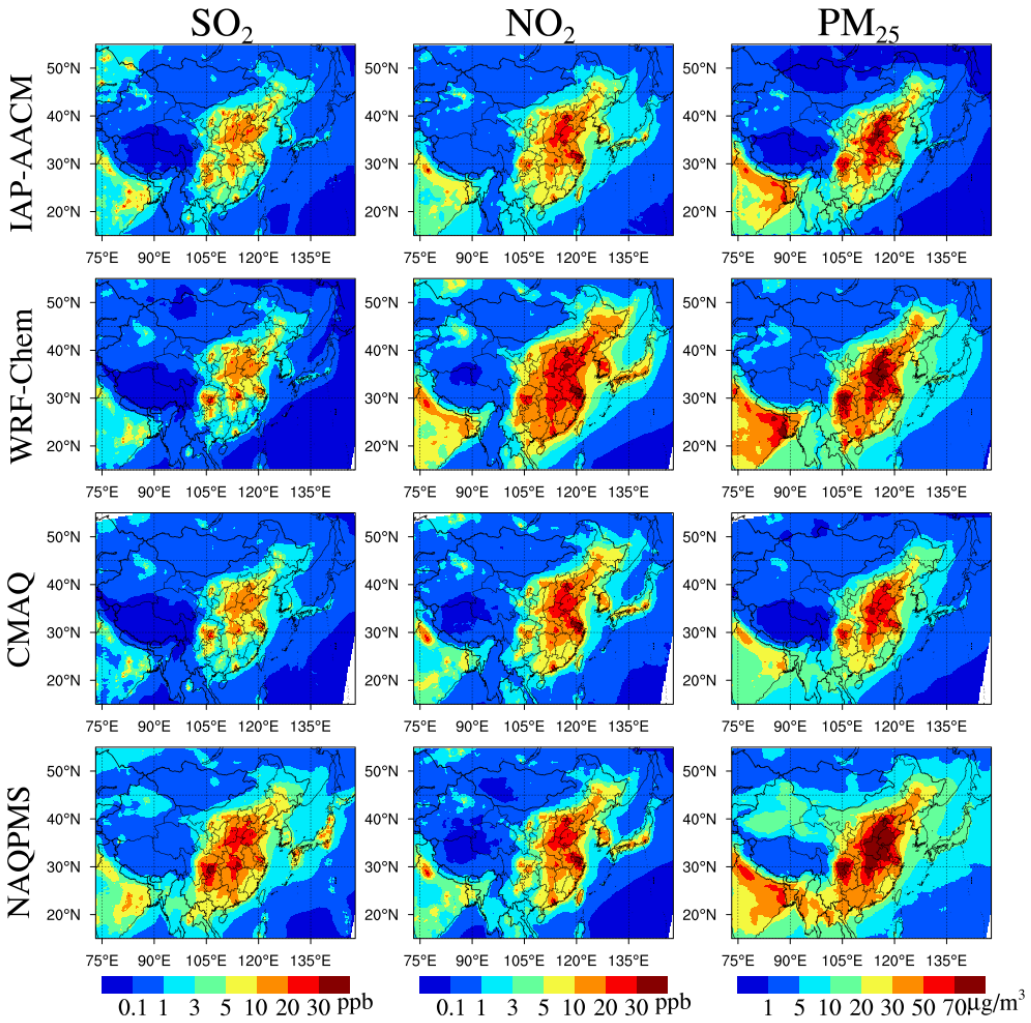

Fig. 12. Annual surface distributions from nested IAP-AACM compared with regional models from MICS-Asia. Each row from top to bottom represents IAP-AACM, WRF-Chem, CMAQ and NAQPMS respectively. The left column is SO_2 (ppb), the middle column is NO_2 (ppb) and the right column is $PM_{2.5}$ (μg m^{-3}).

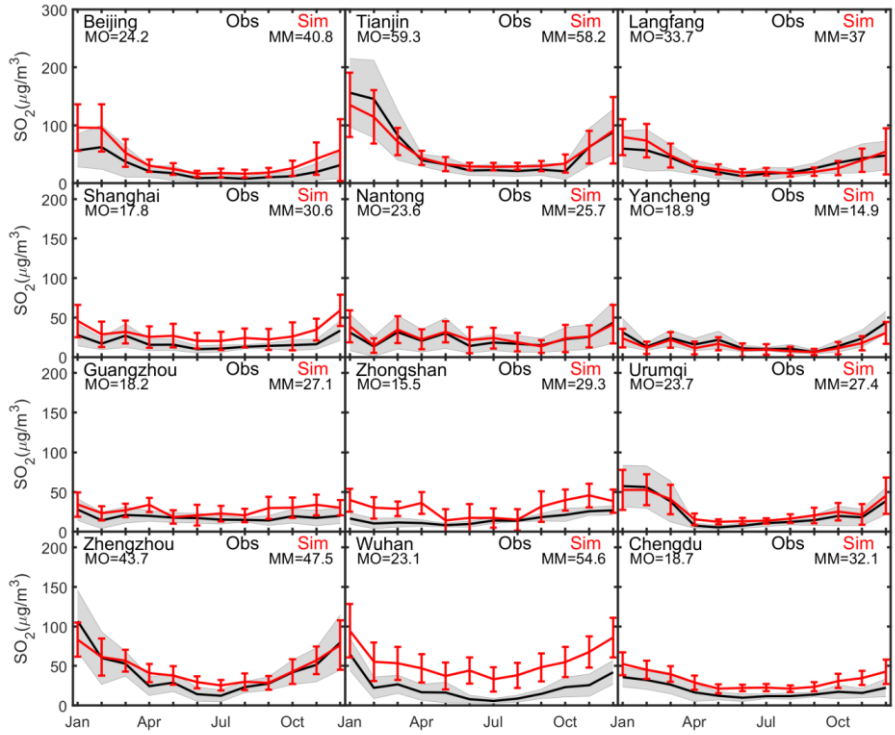

Fig. 13. Mean seasonal variation of SO_2 (μg m^{-3}) over China. The black line and red line represent monthly mean concentration of city-averaged observation and simulation respectively. Gray shaded areas and red vertical bars show 1 standard deviation over the sites for observations and for model results, respectively. MO and MM stand for annual mean concentration of observation and simulation respectively.

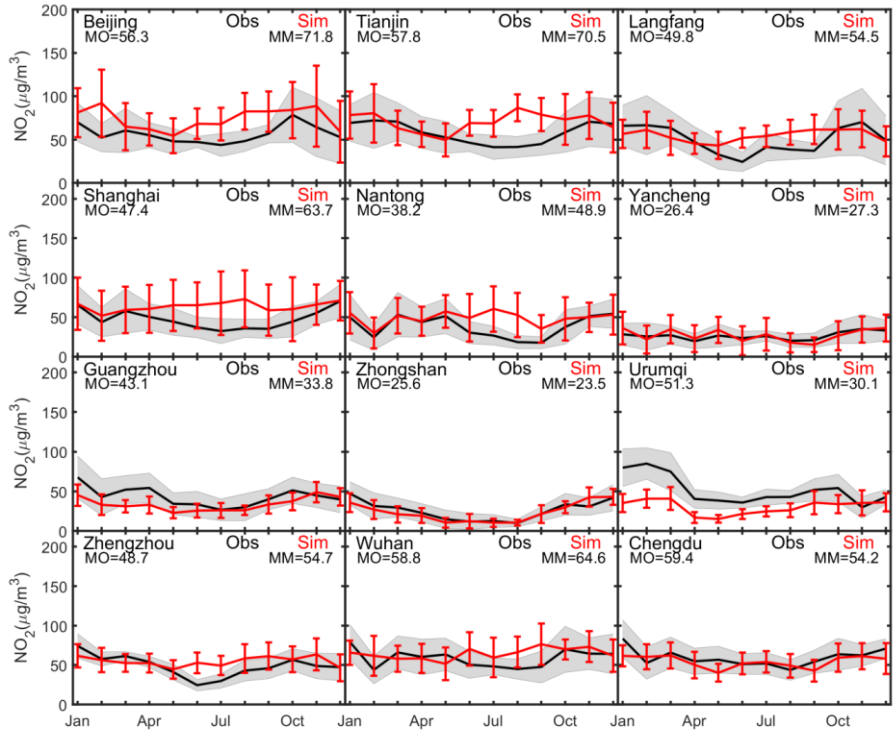

Fig. 14. The same as Fig. 15, except the pollutant is NO_2.

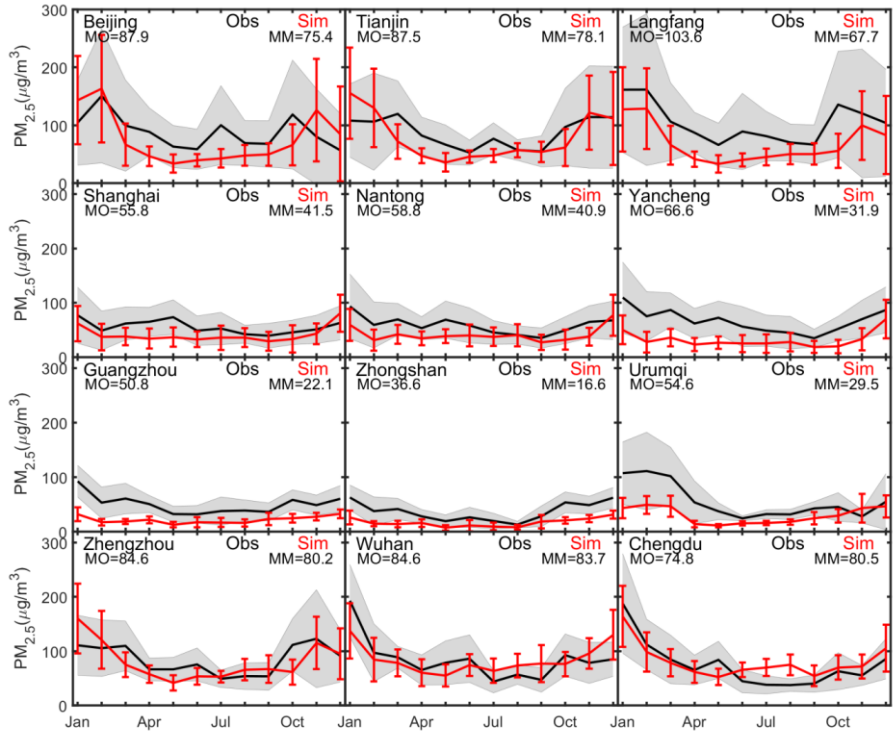

Fig. 15. The same as Fig. 15, except the pollutant is $PM_{2.5}$. The components of $PM_{2.5}$ includes primary $PM_{2.5}$, BC, POA, SOA and SNA.

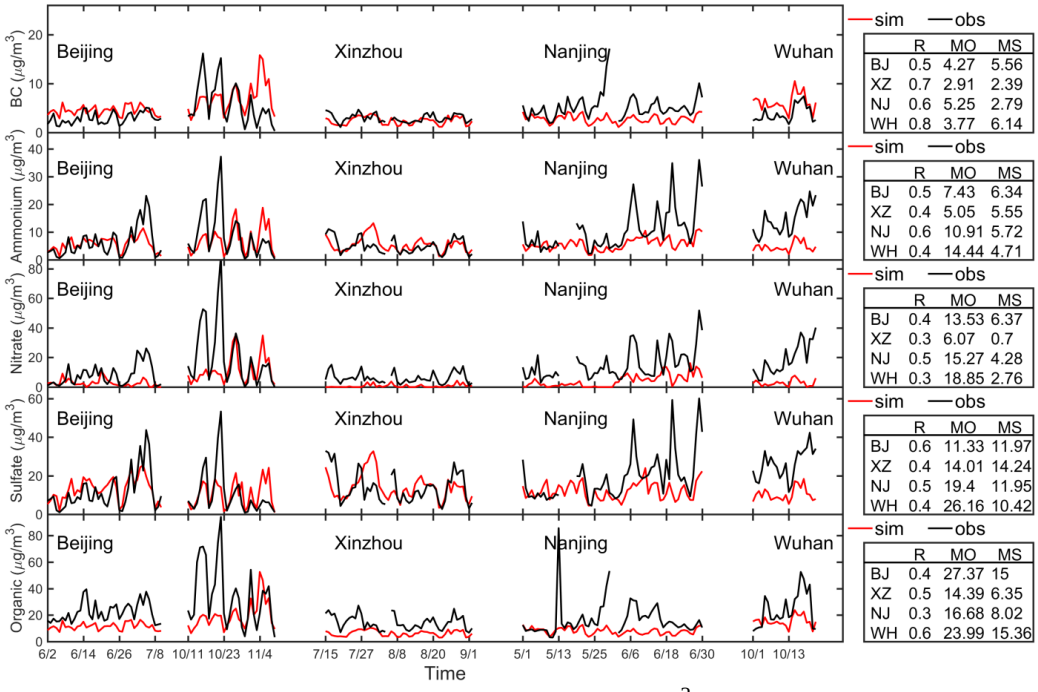

Fig. 16. Daily variation of aerosol components (μg m^{-3}) over China. The black line and red line represent daily mean concentration of city-averaged observation and simulation respectively. BJ, XZ, NJ and WH mean Beijing, Xinzhou, Nanjing and Wuhan respectively. R, MO and MM stand for correlation coefficient, mean concentration of observation and model respectively.

Tables

Table 1. Emissions used in IAP-AACM

Database	Abbreviation	Base year	Source type	Reference
Hemispheric Transport of Air Pollution version2	HTAP-v2	2010	Anthropogenic	Janssens-maenhout et al., 2015
Global Fire Emissions Database version4	GFED-v4	2010	Biomass burning	Randerson et al., 2015
Model of Emissions of Gases and Aerosols from Nature–Monitoring Atmospheric Composition and Climate	MEGAN-MACC	2010	Biogenic	Sindelarova et al., 2014
Regional Emission inventory in Asia	REAS	2001	Soil (NOx)	Yan et al., 2005
Precursors of Ozone and their Effects in the Troposphere	POET	2000	Ocean (VOCs)	Granier et al., 2005
Global Emission InitiAtive	GEIA	Average of 1983 ~ 1990	Lightning (NOx)	Price et al., 1997

Table 2. Summary of statistical of annual and seasonal meteorology in the nested domain compared with NCDC sites. Seasons are defined as spring (March–May), summer (June–August), fall (September–November), and winter (December–February). MO, MM, RMSE and R represents mean value of observation, mean value of model, root mean square error and correlation coefficients respectively. T_2, W_{10} and RH_2 represent temperature at 2m (℃), wind speed at 10 m (m/s) and relative humidity at 2m (%) respectively.

	Period	MO	MM	MB	RMSE	R
T_2	2014	17.6	17.5	-0.1	1.8	0.98
	Spring	16.3	16.2	-0.1	1.9	0.97
	Summer	24.3	24.0	-0.3	2.0	0.93
	Autumn	17.2	17.0	-0.2	1.7	0.97
	Winter	9.5	9.5	0.0	1.7	0.96
W_{10}	2014	3.1	2.5	-0.6	1.5	0.53
	Spring	3.2	2.7	-0.5	1.8	0.61
	Summer	2.9	2.1	-0.8	1.9	0.48
	Autumn	3.0	2.3	-0.7	1.7	0.53
	Winter	3.1	2.4	-0.7	1.8	0.56
RH_2	2014	64.8	61.7	-3.1	12.3	0.84
	Spring	58.5	56.2	-2.3	12.6	0.86
	Summer	71.2	68.0	-3.2	11.7	0.86
	Autumn	68.1	64.0	-4.1	11.7	0.83
	Winter	61.4	58.6	-2.8	13.2	0.76

Table 3. Summary of the site observation datasets

Dataset	Site number	Year	Region of sites located	Observed species
WDCGG	131	2014	Global	CO, O_3, SO_2, NO_2
EANET	41	2014	East Asia	SO_2, NO_2, O_3, $PM_{2.5}$, sulfate, nitrate, ammonium
EMEP	46	2014	Europe	$PM_{2.5}$, BC, OC, sulfate, nitrate, ammonium
IMPROVE	23	2014	America	$PM_{2.5}$, BC, OC, sulfate, nitrate, ammonium
EPA	93	2014	America	SO_2, NO_2, $PM_{2.5}$
CAWNET	13	2006	China	BC, OC
CNEMC	89	2014	China	CO, O_3, SO_2, NO_2, PM_{10}, $PM_{2.5}$
Others	4	2014	China	BC, OM, sulfate, nitrate, ammonium

Table 4. Global budgets for DMS, SO_2 and sulfate

Species		IAP-AACM	Other models[a]
DMS	Sources (Tg S yr^{-1})	22.8	
	Emission	22.8	10.7~23.7
	Sinks (Tg S yr^{-1})	22.8	
	Dry deposition	0.0	
	Oxidation	22.8	
	Burden (Tg S)	0.19 ↑[b]	0.02~0.15
	Lifetime (days)	3	0.5~3.0
SO_2	Sources (Tg S yr^{-1})	77.1	
	Emission	54.3 ↓[b]	63.4~94.9
	DMS oxidation	22.8	10.0~25.6
	Sinks (Tg S yr^{-1})	77.1	
	Dry deposition	28.0	16.0~55.0
	Wet deposition	0.0	0~19.9
	Gas-phase oxidation	19.3	6.1~22.0
	Aqueous-phase oxidation	29.8	24.5~57.8
	Burden (Tg S)	0.63	0.2~0.69
	Lifetime (days)	3.0 ↑[b]	0.6~2.6
Sulfate	Sources (Tg S yr^{-1})	50.5	
	Emission	1.4	0~3.5
	Gas-phase oxidation	19.3	6.1~22.0
	Aqueous-phase oxidation	29.8	24.5~57.8
	Sinks (Tg S yr^{-1})	50.5	
	Dry deposition	2.9	0.8~18.0
	Wet deposition	47.6	34.7~61.1
	Burden (Tg S)	0.82	0.38~1.07
	Lifetime (days)	5.9	3.0~7.9

[a] including Liu et al. (2005), Lee et al. (2015), and those listed in Liu et al. (2005), the range of sulfate is also refer to the GISS-TOMAS (Lee et al., 2010), ACCMIP (Lee et al., 2013) and the AeroCom (Textor et al., 2006) results.

[b] outside the range of other models

Table 5. Global budgets for carbonaceous aerosol

Species		IAP-AACM	Other models[a]
BC	Sources (Tg yr^{-1})	7.42	
	Emission	7.42	7.4~19.0
	Sinks (Tg yr^{-1})	7.42	
	Dry deposition	1.01	0.3~4.6
	Wet deposition	6.41	3.8~13.7
	Burden (Tg)	0.13	0.08~0.59
	Lifetime (days)	6.4	3.3~9.4
OM[b]	Sources (Tg yr^{-1})	56.7	50~216
	Emission	48.7	34~144
	Chemical production	8.0	7.8~120
	Sinks (Tg yr^{-1})	56.7	
	Dry deposition	6.79	2~36
	Wet deposition	49.9	28~209
	Burden (Tg)	1.16	0.7~3.8
	Lifetime (days)	7.4	3.5~9.2

[a] including Liu et al. (2005), Lee et al. (2010), Lee et al. (2013), Lee et al. (2015), Textor et al. (2006), and those listed in Liu et al. (2005).

[b] the convert factor from OC to OM is 1.7 in IAP-AACM.

Table 6. Summary of statistics for global and nested domains. D1 and D2 represent results of domain 1 and domain 2, respectively. City Ave means average over all the cities.

Species	City	R		RMSE (μg m^{-3})		MB (μg m^{-3})		NMB	
		D1	D2	D1	D2	D1	D2	D1	D2
$PM_{2.5}$	Beijing	0.69	0.70	54.28	55.65	-12.33	-16.89	-0.14	-0.19
	Tianjin	0.67	0.72	46.63	46.51	-11.00	-13.27	-0.13	-0.15
	Langfang	0.72	0.79	66.02	65.22	-28.58	-38.34	-0.28	-0.37
	Shanghai	0.71	0.71	29.51	27.99	-18.23	-16.00	-0.33	-0.29
	Nantong	0.69	0.75	31.46	29.70	-18.32	-17.84	-0.31	-0.30
	Yancheng	0.74	0.80	45.52	43.30	-35.60	-33.99	-0.53	-0.51
	Guangzhou	0.43	0.63	38.75	36.91	-29.91	-29.39	-0.59	-0.58
	Zhongshan	0.51	0.76	26.16	26.77	-16.08	-20.38	-0.44	-0.56
	Urumqi	0.31	0.50	59.32	48.10	-38.40	-25.88	-0.70	-0.47
	Zhengzhou	0.59	0.63	41.98	43.05	0.70	-7.30	0.01	-0.09
	Wuhan	0.57	0.64	44.49	42.28	-11.32	-12.09	-0.13	-0.14
	Chengdu	0.76	0.77	37.18	36.14	5.23	-0.19	0.07	0.00

	City Ave	0.68	0.70	49.86	51.07	-10.01	-10.95	-0.11	-0.12
SO_2	Beijing	0.87	0.89	26.99	25.00	21.32	16.58	0.88	0.68
	Tianjin	0.85	0.85	35.45	29.51	-10.96	-1.10	-0.18	-0.02
	Langfang	0.74	0.76	24.65	18.90	11.49	3.38	0.34	0.10
	Shanghai	0.50	0.75	38.48	18.10	30.43	12.76	1.71	0.72
	Nantong	0.69	0.78	13.55	12.08	-0.23	2.17	-0.01	0.09
	Yancheng	0.78	0.83	9.75	8.79	-4.29	-4.02	-0.23	-0.21
	Guangzhou	0.26	0.40	10.42	14.96	-0.96	8.86	-0.05	0.49
	Zhongshan	0.59	0.33	7.33	21.65	1.65	13.74	0.11	0.88
	Urumqi	0.63	0.60	23.04	20.01	-11.88	3.68	-0.50	0.16
	Zhengzhou	0.79	0.82	24.51	20.06	12.34	3.84	0.28	0.09
	Wuhan	0.70	0.48	18.72	40.28	12.03	31.47	0.52	1.36
	Chengdu	0.52	0.60	48.52	17.61	44.44	13.33	2.37	0.71
	City Ave	0.76	0.83	31.50	27.35	5.18	7.74	0.12	0.19
NO_2	Beijing	0.48	0.68	26.00	26.82	11.98	15.68	0.21	0.28
	Tianjin	0.41	0.51	26.24	27.39	9.88	13.02	0.17	0.23
	Langfang	0.39	0.53	33.84	23.83	19.60	4.91	0.39	0.10
	Shanghai	0.57	0.56	29.28	32.17	8.79	16.79	0.19	0.35
	Nantong	0.60	0.59	21.86	24.11	3.63	10.69	0.10	0.28
	Yancheng	0.44	0.49	18.33	16.53	-1.55	1.78	-0.06	0.07
	Guangzhou	0.40	0.51	28.34	20.28	-20.41	-9.19	-0.47	-0.21
	Zhongshan	0.63	0.70	13.47	12.51	-3.01	-2.06	-0.12	-0.08
	Urumqi	0.24	0.41	41.73	30.31	-35.18	-21.39	-0.69	-0.42
	Zhengzhou	0.32	0.44	23.68	18.75	13.65	5.97	0.28	0.12
	Wuhan	0.25	0.22	25.36	28.39	5.77	6.16	0.10	0.10
	Chengdu	0.31	0.43	27.26	20.77	-18.88	-5.84	-0.32	-0.10
	City Ave	0.44	0.60	26.05	26.92	10.82	13.99	0.19	0.25